Imperial College London

Transition In Stratified Shear Flows: Linear Stability Analysis With A Shear And Stratification Inalignment

Final Year Project

Academic Supervisor: Dr. Yongyun Hwang
Academic Second Marker: Prof. Sergei Chernyshenko
Department: Aeronautics
Academic year: 2019/2020

Student: Joel Outschoorn
Date: May 21, 2020

Abstract

- Stratified shear flow transitional analysis.
- Linear Stability Analysis of stratified plane Couette and plane Poiseuille flows where the shear and stratification are not aligned.
- Inalignment from theta.
- Stability/instability found when theta = ...
- Unstable eigenvalues.

Contents

Acknowledgements

A handful of academics played a vital role in my completion of this project, firstly and most importantly I want to express my gratitude to Dr. Yongyun Hwang for his complete supervision throughout this year, and I must mention Professor Sergei Chernyshenko for his contributions towards insight in the project at the Interim Assessment. I would also like to thank my academic tutor, Dr. Thulasi Mylvaganam for her unconditional guidance and care. A large number of members of the Imperial community made my time here a true pleasure, and provided a strong and unconditional support network. In particular I would like to thank Jackie O'Neill and Dr. Errikos Levis.

List of Figures

List of Tables

Nomenclature

Acronyms

DNS	Direct Numeric Simulation	
HSA	Hydrodynamic Stability Analysis	
LSA	Linear Stability Analysis	
pBj	Plane Bickley jet	
pCf	Plane Couette flow	
pPf	Plane Poiseuille flow	

Non-Dimensional Parameters

Re	Reynolds number	$\frac{\rho U L}{\mu}$
F_h	Horizontal Froude number	$\frac{U}{N L_h}$
F_v	Vertical Froude number	$\frac{V}{N L_v}$

List of Symbols

ρ	Fluid density	kg/m^3
U	Fluid mean velocity	m/s

Chapter 1

Introduction and Motivations

Shear and density stratification are common features of Earth flow fields, these are fluids that have significant velocity and density gradients. While typical aeronautical practices do not encounter stratified flows, these fluid structures are ubiquitous in other applications, such as oceanography and meteorology.

Fluids with density stratification are common in the atmosphere and oceans. In the ocean, from gravitational influences, the fluid is more saturated with salts at lower depths which creates a density stratified fluid. As for the atmosphere, it is known that the air is density stratified under gravity. The International Standard Atmosphere (ISA) models the stratification by splitting the atmosphere into layers, each with its own density gradient. The stratification modifies flow behaviours significantly that makes it a field of interest.

Shear instability is one of the famous fields of research in fluid dynamics. The evolution of shear flows has been broadly studied due to its industrial and geophysical interest. However, research in the effects of an applied uniform density stratification on the linear growth of shear instability is still absent. The influence of stable stratification is agreed to be stabilising in the case of shear and stratified alignment. Likewise, the study of orthogonality has been extensively investigated (REFERENCE FACCHINI AND LUCAS). In the analysis presented here, the examination of a stratified plane shear flow is carried out for the situation when the shear and stratification are not aligned.

The transition of these stratified structures to turbulence in shear flows has not been well understood. The fundamental aim will be to study the early stage of transition in stratified shear flows using linear dynamical systems theory.

The density variations strongly influence the fluid dynamics particularly the stability of such flows. Important parameters which quantify stratified fluids are the Brunt–Väisälä frequency, N, and the Froude number, F_h. These constants determine the strength of the density stratification and their significance will be discussed in Chapter 3. The shear flows that were investigated were mainly the plane Couette flow (pCf), Figure 1.1(a), and plane Poiseuille flow (pPf), Figure 1.1(b). pCf arises from two plates moving in opposite directions which creates a linear velocity gradient, whereas pPf are formed by a downstream pressure drop with non-moving plates and the fully developed flow structure would give rise to a parabolic velocity profile. The shear and stratification give rise to velocity and density gradients respectively. The significant field of interest in this report is for when this velocity and density gradient are not in the same plane. This occurs in the presence of a shear and stratification inalignment. The flow structures that will be investigated in the following Chapters in a plane shear flow that is tilted by an inalignment angle, *theta*, with respect to a linear density gradient plane.

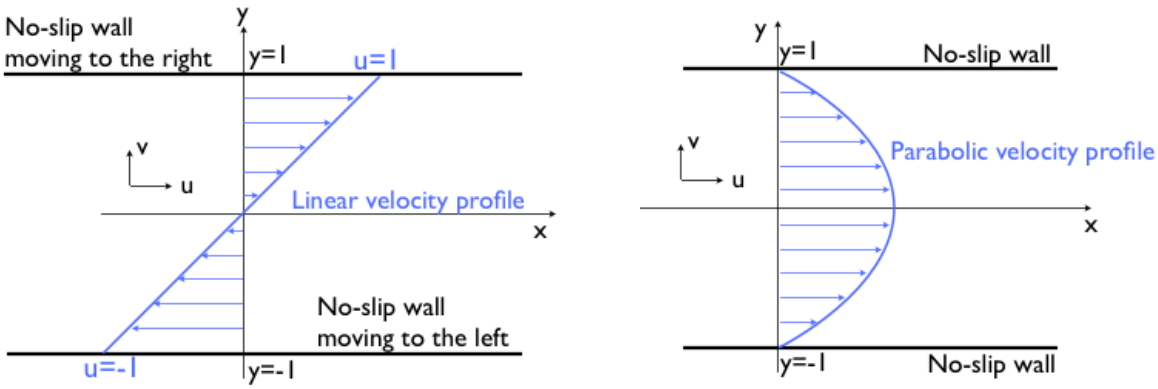

(a) Plane Couette flow (pCf).

(b) Plane Poiseuille flow (pPf).

Figure 1.1: Shear flow structures of interest.

To illustrate the various observations, this report is organised as follows. Chapters 3 and 2 provides a breakdown of the fundamental theories that will be applied, with Chapter 3 focusing on understanding stratified flows while Chapter 2 will summarise the fluid dynamic analysis. Chapter 4 presents the main goals of the project. Chapter 5 provides the formulation of the numerical simulations and defines the various parameters of interest. Chapter 6 presents the numerical method that was implemented and analysis on the reliability of the chosen method. Chapter 7 provides the main results and discussions from the analysis and finally Chapter 8.1 considers potential further studies and the main conclusions.

Chapter 2

Literature Review: Hydrodynamic Stability

Here we endeavour to demonstrate a brief introduction on the theories of Linear Stability Analysis (LSA), a branch of Hydrodynamic Stability Analysis, for parallel shear flows. The information for LSA was largely provided through the lecture notes REFERENCE HERE.

Hydrodynamic Stability Analysis (HSA) is the branch of fluid dynamics investigating the transition of laminar fluid flows to turbulence. Transition is sensitive to external noise and disturbances leading to dramatic changes in the flow field. The governing equations of fluid dynamics (in the unstratified case would be the Navier Stokes equations) produces basic laminar flow structures as a basic solution. In some cases, these laminar states are prone to instabilities due to certain critical conditions. The unstable modes causes the flow to evolve into more complicated flow patterned/unpatterned (turbulent) states. The study of HSA is important mainly because it provides an explanation as to the discrepancy between analytical solutions that satisfy the governing equation and what is naturally occurring or observable in experiments.

HSA allows fluid structures to be modelled as a system, with the known solution in the space-time field as the basic equilibrium flow. When the system is deviated from this equilibrium state, the system stability characterises whether the flow arrangement will return to its original basic flow or whether the flow field will break down into turbulent structures. The formal definition of stability is in the Lyapunov sense, however we will assume the perturbations are infinitesimal. It must be pointed out that nonlinear or secondary instabilities do hold significance to destabilise flows. Nevertheless, previous work has proven that primary linear stability first govern the flow behaviour before any global or non-linear stability.

The main analysis that shall be presented in this report is fundamentally the solutions to an eigenvalue problem, where the eigenspectra determines the base flow stability and the eigenfunctions give the shape of the state perturbations.

2.1 Linear Stability Analysis

This branch of HSA investigate the initial onset of these instabilities and the critical conditions which induces them. The dynamics of perturbations from a fully developed equilibrium base flow is examined. The instability is caused if these perturbations were to exhibit signs of temporal growth. The mathematical definition for stability is the supression of these perturbations.

The linear stability we shall consider will be referenced from two-dimensional parallel shear flows. Following the fundamental steps of famous Orr-Sommerfeld/Squire system of equations which governs the stability of uni-directional viscous fluids.

The main steps of linear stability analysis is presented below:

- Introduce the base flow velocity profile, in our case is pCf and pPf profiles. Decompose the profile into the equilibrium flow and a perturbation.
- Substitute this velocity profile into the governing equations of motion. Apply linearisation by neglecting higher order squared terms.
- Next develop a normal mode solution which will be of an exponential form with the spatial and temporal terms. Substitute this solution into the linearised governing equations.
- Following certain manipulations for the Orr-Sommerfeld/Squire equations which will reduce it into a finalised eigenvalue system.

The complete derivation of the stratified eigenvalue problem is presented in Chapter 5.

2.1.1 Theory on Absolute and Convective Instability

Briefly we shall discuss the significance of the types of linear instabilities typically found. Considering the linear stability of an open flow, if all infinitesimal perturbations decay over a domain in time and space the flow is linearly stable. Many flows are open flows, hence disturbances and external excitations can be washed downstream hence the flow should always be stable, granted there is no continuous perturbation. This notion led to the definitions of absolute and convective instabilities. These distinguish between perturbation stabilities that would be convected away or those that would remain and grow. The formal definitions for Convective and Absolute Instabilities are:

- Linearly Convectively Unstable: Disturbances that grow in space and time but are ultimately advected away from the region of interest by the freestream.
- Linearly Absolutely Unstable: Disturbances that grow in space and time but remain at the source.

Mathematical Definition for Absolute and Convective Stability

To determine the type of stability of the eigenmodes, one is concerned with the complex frequency, $\omega = \omega_r + i\omega_i$, which will be defined and discussed in Section 5. The stability criterion depends on the growth rate, ω_i:

- If $\omega_{i,0} > 0$ and $\omega_{i,max} > 0$ then the system is Absolutely Unstable.
- If $\omega_{i,0} < 0$ and $\omega_{i,max} > 0$ then the system is Absolutely Stable and Convectively Unstable.
- If $\omega_{i,0} < 0$ and $\omega_{i,max} < 0$ then the system is Absolutely Stable.

Our analysis does not concern ourselves too much on the types of instabilities occurring but more the conditions of stability and the influence of the tilt on the base flow behaviour.

Chapter 3

Literature Review: Stratified Flows

This Chapter aims to introduce the concept of stratification and review the main findings of stability analysis carried out by past researchers into the transition of stratified shear flows, mainly concerning the pCf and plane Bickley jets (pBj). These literature provided the validation means for the developed numerical solver. Stratified shear flows are simply fluids with a density variation. Therefore, there exists a density profile as well as the shear velocity profile. Means to quantify stratified fluids is described in Section 3.1, while their governing system of equations will be discussed in Section 3.2.

3.1 Non-Dimensional Parameters

Stratification is quantified using the Brunt–Väisälä frequency, N, where increasing this parameter strengthens the density gradient. The Froude number, F, and the bulk Richardson number, Ri, are dimensionless parameters defining the density gradient strength, where $Ri = F_h^{-1}$.

$$F = \frac{u}{Nl} \tag{3.1.1}$$

The Froude number, determined by Equation (3.1.1), is more typically used in existing research, where u is the flow velocity and l is the characteristic length. It quantifies the stratification strength based from the Brunt-Vaisala frequency. For two-dimensional flows, one can define both F in the horizontal, F_h, and vertical, F_v, direction using the velocities (U, V) and lengths (L_h, L_v) representing the horizontal and vertical directions. Since we are working with parallel base flows, we only concern ourselves with $F_h = (\frac{U}{NL_h})$. The criteria for strongly stratified flows are those with $F_h \leq 1$, with stronger density gradients achieved by reducing F_h.

3.2 Governing Equations

The governing equations that model stratified fluids are the Navier-Stokes equation under the Boussinesq approximation. Here a linear stratification is applied to the momentum eqautions via a gravity gradient acting downwards. Therefore, the density decreases linearly as you move up the vertical direction. The Boussinesq approximation also models the density transport, however these density variations are assumed to be very small. Hence, an incompressible flow assumption is still valid. The governing system is shown in Equations (3.2.1) to (3.2.2) below:

$$\frac{\partial \mathbf{u}^*}{\partial t^*} + (\mathbf{u}^* \cdot \nabla)\mathbf{u}^* = -\frac{\nabla p^*}{\rho_0^*} + \nu^* \nabla^2 \mathbf{u}^* - \frac{\rho'^* g^*}{\rho_0^*}\hat{\mathbf{Y}} \tag{3.2.1}$$

$$\frac{\partial u^*}{\partial x^*} + \frac{\partial v^*}{\partial y^*} + \frac{\partial w^*}{\partial z^*} = 0 \tag{3.2.2}$$

$$\frac{\partial \rho'^*}{\partial t^*} + (\mathbf{u}^* \cdot \nabla)\rho'^* = K^* \nabla^2 \rho'^* \tag{3.2.3}$$

Equations (3.2.1) represent the momentum terms where $\mathbf{u}(= (u, v, w))$ is the three-dimensional velocity vector, p is the pressure state, ν the kinematic viscosity, ρ' and ρ_0 are the density perturbation and reference density respectively and g is the gravity which provides us our stratification. $\hat{\mathbf{Y}}$ simply represents the direction of the density gradient. Equation (3.2.2) illustrates the continuity equation, where an incompressible assumption has already been applied. Finally, Equation (3.2.3) presents the density transport given from the Boussinesq approximation, where K is the density diffusivity. Note that the (*) represents dimenioned variables, it is useful to non-dimensionalise these equations in order to reduce error. The use and manipulation of these equations will be illustrated in Chapter 5.

3.3 Past Work On Stratified Shear Flow Stability

REFERENCE ALL THE STRATIFICATION PAPERS Initially, to understand the notion of stratified flows, PAPER 1, was reviewed. The main points were conveying the idea that strongly stratified fluids would arrange itself into layered structures with density interfaces. This paper mainly discussed the manipulations to the governing equations to provide dimensionless forms and the significance of the domain sizes of the control volume.

There has been a considerable amount of work on the stability of stratified shear flows with spanwise stratification (shear and stratified orthogonality). The general configuration of these flow structures is shown in Figure 3.1. PAPER 2 investigates the effect of stable spanwise stratification on the pCf. The main results showed how turbulent flows illustrate near-wall layering. Moreover, when N suppresses turbulence, the linear instabilities lead to ordered nonlinear states with the possibility of secondary shear instablities. The three-dimensional stability of spanwise stratified shear flows was investigated in PAPER 4. Here, they found that the Squire theorem where the most unstable perturbation in homogeneous fluids is always two-dimensional does not apply for stably stratified fluids. They found that the stronger the stratification, the smaller the vertical scales that can be destabilised.

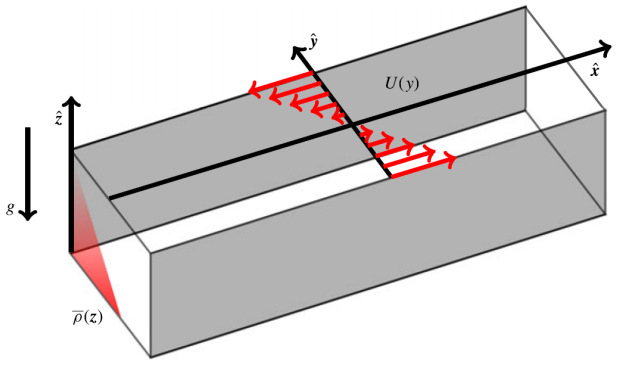

Figure 3.1: Sketch of stratified pCf with a spanwise stratification from PAPER 3. Note that $U(y)$ represents the fully developed shear velocity profile, $\bar{\rho}(z)$ represents the density profile and ($\hat{\mathbf{x}}$,$\hat{\mathbf{y}}$,$\hat{\mathbf{z}}$) is the streamwise, streamnormal and spanwise directions respectively. g is the gravity vector providing the stratification.

PAPER 3 provided the means of validation for the developed LSA Solver. Facchini presents the analysis of the pCf with orthogonal stratification. They performed LSA on the described fluid structure, along with non-linear Direct Numeric Simulations (DNS) and experimental data for validation. The stability was characterised by the Reynolds number, Re and F_h. The main result was that the flow becomes unstable for moderate values of $Re \geq 700$ and for $F_h \approx 1$. The instability is induced from a wave resonant mechanism, known in channel flows.

3.4 Past Work On Shear Stratification Inalignment

PAPER 5 carried out analysis on a tilt angle between the stratification and shear. The analysis was on a two-dimensional pBj with a gravity-induced stratification plane as shown in Figure 3.2. For the aligned case the condition for stability is based on $Ri \geq 1/4$. However, in the inaligned case the pBj is found to always be unstable for all F_h. The fundamental result was that aligning stratification with shear provides stabilisation. This is a known result as the stratification inhibits vertical growth of perturbations from the density gradient, hence the flow relaminarises following deviations. Once inaligned, this induces shear flow instabilities.

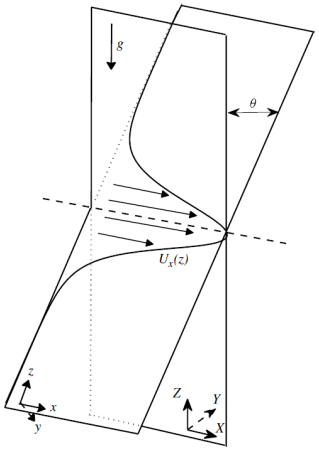

Figure 3.2: Sketch of the base flow (pBj) inaligned to the stratification plane (provided by g) by angle θ from PAPER 5. $U_x(z)$ is the shear velocity profile and there are two coordinate systems where (x, y, z) is the shear plane and (X, Y, Z) is the stratification plane.

Chapter 4

Project Aims and Assumptions

The fundamental goal in a larger context is working towards to a complete understanding of density stratification with a tilted plane shear flow. In the examined work, we look to study the effect of this inclination angle on the linear properties of the shear instability. This project does not mean to achieve a finalised picture of the flow physics but is the first steps towards a thorough and clear-cut understanding. Future work will be required to build on the outcomes of this project to build towards a complete understanding and as stated earlier we shall limit ourselves to linear analysis.

4.1 Assumptions and Approximations

The basis of the presented work will be on linear stability analysis as we concern ourselves with the onset of exponential growth of perturbations from a fully developed base flow. Linear stability analysis first governs the local absolute instability before transitioning to patterned or turbulent structures. From calculation of the onset of instabilities, one should be able to recreate trends similar to experimental observation. The fundamentals of LSA requires us decouple our state parameters into an equilibrium profile plus a perturbation term. Our concern is with the evolution of this perturbation term and to investigate the particular conditions that may suppress or destabilise these deviations from the laminar base flow.

The main assumptions that will shall implement is a fully developed parallel base flow with only a velocity gradient in the vertical direction, U(y). Hence the base flow will be a two-dimensional plane fluid structure. The stratified plane will be derived from a gravitational force which will produce a linear density gradient. The tilted shear flow will produce three-dimensional turbulent structures. Furthermore, the common assumptions of no-slip shear plane boundaries and impenetrable walls are implicitly implied in the project. Despite working with a density gradient, the density transport in the streamwise direction is assumed to be infinitesimal, hence we shall incorporate an incompressible fluid assumption. As a typical application of stratified flows is within oceans, this is a valid assumption.

4.2 Aims and Objections

The presented work aims to provide a more quantitative and theoretical understanding on the effect of inaligned stratification to shear flow stability and the threshold conditions to which the flow remains stable. In particularly,, it is well known that, in unstratified case, the pCf is always linearly stable and the pPf has a critical Re of 5772 as displayed in REFERENCE. Hence, the influence of introducing a density gradient will be examined in comparison to the unstratified and the aligned stratification cases. Likewise, we would like to observe the destabilising mode that happens at high stratification when they are not aligned.

Chapter 5

Theoretical Framework

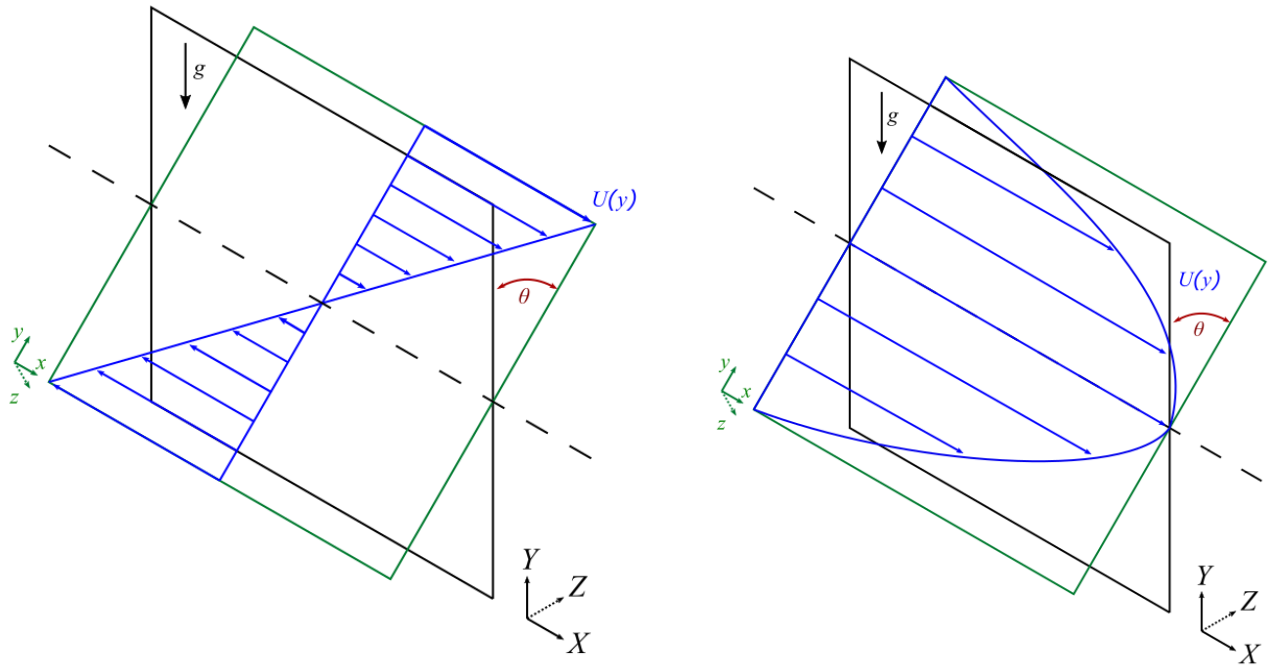

(a) Plane Couette flow (pCf).

(b) Plane Poiseuille flow (pPf).

Figure 5.1: Stratified shear flow inalignment by angle θ.

This chapter derives the stratified system of equations that will be solved by LSA, starting from the governing equations with the Boussinesq approximation that was introduced in Section 3.2. The derivation largely follows the steps of the famous Orr-Sommerfeld/Squire system for parallel shear flows. The stratified fluid structure is visualised in Figure 5.1, showing both investigated shear flows; the pCf (Figure 5.1(a)) and the pPf (Figure 5.1(b)).

5.1 Formulation

The pCf base flow is generated by two parallel moving walls with opposite velocities, while the pPf base flow is generated by a downstream pressure gradient with non-moving no-slip walls which generates the parabolic profile. The shear flow is tilted to the stratification plane by angle θ.

5.1.1 Coordinate System

The initial laminar shear flow is assumed to be two-dimensional, where the shear plane is confined to $(\hat{\mathbf{x}}, \hat{\mathbf{y}}, \hat{\mathbf{z}})$ and the stratification plane is confined to $(\hat{\mathbf{X}}, \hat{\mathbf{Y}}, \hat{\mathbf{Z}})$. We use the $(\hat{\cdot})$ symbol define unit vectors in the respective direction. We denote $\hat{\mathbf{x}}$ as the streamwise direction, $\hat{\mathbf{y}}$ as the streamnormal direction and $\hat{\mathbf{z}}$ as the spanwise direction. The variable g denotes gravity, which has vector $\mathbf{g} = (0\hat{\mathbf{X}} - g\hat{\mathbf{Y}} + 0\hat{\mathbf{Z}})$, while the blue arrows sketch the shape of the constant shear velocity profile, which only changes in the streamnormal direction, $U(y)$. The tilt angle θ is with respect to the centre of each plane, where the shear plane is inaligned to the stratification plane. This tilt angle gives the transformations between coordinate systems as:

$$(\hat{\mathbf{X}}, \hat{\mathbf{Y}}, \hat{\mathbf{Z}}) = (\hat{\mathbf{x}}, \hat{\mathbf{y}}\cos\theta - \hat{\mathbf{z}}\sin\theta, \hat{\mathbf{y}}\sin\theta + \hat{\mathbf{z}}\cos\theta) \tag{5.1.1}$$

5.1.2 Governing Equations

For clarity, we reintroduce our system of equations under the Boussinesq approximation, where (*) represents dimensioned variables:

$$\frac{\partial \mathbf{u}^*}{\partial t^*} + (\mathbf{u}^* \cdot \nabla)\mathbf{u}^* = -\frac{\nabla p^*}{\rho_0^*} + \nu^* \nabla^2 \mathbf{u}^* - \frac{\rho'^* g^*}{\rho_0^*}\hat{\mathbf{Y}} \tag{5.1.2}$$

$$\frac{\partial u^*}{\partial x^*} + \frac{\partial v^*}{\partial y^*} + \frac{\partial w^*}{\partial z^*} = 0 \tag{5.1.3}$$

$$\frac{\partial \rho'^*}{\partial t^*} + (\mathbf{u}^* \cdot \nabla)\rho'^* = K^* \nabla^2 \rho'^* \tag{5.1.4}$$

5.1.3 Non-dimensionalisation

For convenience, one should look to non-dimensionalise the governing equations. This can be done in many ways as analysed in PAPER 1. The most intuitive way to non-dimensionalise is the use the time-average mean velocity, characteristic length and reference density. This allows us to introduce the important dimensionless parameters Re, F_h and Sc. Next we can also introduce the dimensionless buoyancy $b = \frac{\rho' g}{\rho_0}$.

$$\frac{\partial \mathbf{u}}{\partial t} + (\mathbf{u} \cdot \nabla)\mathbf{u} = -\nabla p + \frac{1}{Re}\nabla^2 \mathbf{u} - \frac{b}{F_h^2}\hat{\mathbf{Y}} \tag{5.1.5a}$$

$$\frac{\partial \mathbf{u}}{\partial t} + (\mathbf{u} \cdot \nabla)\mathbf{u} = -\nabla p + \frac{1}{Re}\nabla^2 \mathbf{u} - \frac{b}{F_h^2}(\cos\theta\hat{\mathbf{y}} - \sin\theta\hat{\mathbf{z}}) \tag{5.1.5b}$$

$$\frac{\partial u}{\partial x} + \frac{\partial v}{\partial y} + \frac{\partial w}{\partial z} = 0 \tag{5.1.6}$$

$$\frac{\partial b}{\partial t} + (\mathbf{u} \cdot \nabla)b = \frac{1}{ReSc}\nabla^2 b \tag{5.1.7}$$

Equations (5.1.5) to (5.1.7) represent the dimensionless version of our original dimensioned system of Equations (5.1.2) to (5.1.4). Note that the momentum Equation (5.1.5a) has the buoyancy applied in the stratification plane, therefore by using (5.1.1), the momentum Equation system can be rewritten as (5.1.5b). A key thing to note is that our density transport equation is now in terms of the dimensionless buoyancy, as shown in (5.1.7). Equation (5.1.6) remains as our continuity expression that already has the

incompressiblity applied to it.

Equations (5.1.5) to (5.1.7) will be taken forward as our systems governing equation system and the derivation of the eigenvalue problem will follow from these equations. The next step is to decouple the equation states $(\mathbf{u}, p, b)$ into a basic solution, $(\mathbf{u}_0, p_0, b_0)$, plus a perturbation term, $(\mathbf{u}', p', b')$. This is shown in Equation (5.1.8). Note that the basic solution for the velocity state is $\mathbf{u}_0 = (U(y), 0, 0)$ with perturbed velocities (u', v', w').

$$\begin{aligned} \mathbf{u} &= \mathbf{u}_0 + \mathbf{u}' \\ p &= p_0 + p' \\ b &= b_0 + b' \end{aligned} \tag{5.1.8}$$

5.1.4 Linearisation

These state solutions are then subbed into the dimensionless governing equations. The perturbed terms are assumed to be infinitesimally small, hence any second order terms are approximated as negligible giving us the linearised governing equations presented below.

$$\frac{\partial u'}{\partial t} + U\frac{\partial u'}{\partial x} + v'\frac{dU}{dy} = -\frac{\partial p'}{\partial x} + \frac{1}{Re}\nabla^2 u' \tag{5.1.9a}$$

$$\frac{\partial v'}{\partial t} + U\frac{\partial v'}{\partial x} = -\frac{\partial p'}{\partial y} + \frac{1}{Re}\nabla^2 v' - \frac{b'}{F_h^2}\cos\theta \tag{5.1.9b}$$

$$\frac{\partial w'}{\partial t} + U\frac{\partial w'}{\partial x} = -\frac{\partial p'}{\partial z} + \frac{1}{Re}\nabla^2 w' + \frac{b'}{F_h^2}\sin\theta \tag{5.1.9c}$$

$$\frac{\partial u'}{\partial x} + \frac{\partial v'}{\partial y} + \frac{\partial w'}{\partial z} = 0 \tag{5.1.10}$$

$$\frac{\partial b'}{\partial t} + U\frac{\partial b'}{\partial x} - (\mathbf{u}' \cdot \nabla)\left(\frac{Y}{F_h^2}\right) = \frac{1}{ReSc}\nabla^2 b' \tag{5.1.11}$$

Equation (5.1.9) illustrates the linearised momentum equations, expressing all the (x, y, z) components and Equation (5.1.10) gives the linearised incompressible continuity expression. The linearised density transport equation, Equation (5.1.11), was derived with the help of LLOYD/HWANG. The Y term is the vertical direction in the stratification plane. To transform the equation into the shear plane, one must use Equation (5.1.1).

5.2 Normal-Mode Solution

The state variables are (u', v', w', p', b'). However, this would create a large system that would have a heavy computational cost. Following the Orr-Sommerfeld/Squire system, we can introduce the wall-normal voriticity, expressed by Equation (5.2.1) below:

$$\eta' = \left(\frac{\partial u'}{\partial z} - \frac{\partial w'}{\partial x}\right) \tag{5.2.1}$$

Hence, some manipulation is required in order to reduce the system to state variables (v', η', b'). Local stability properties are then obtained by considering the perturbed states as a plane wave with the normal mode solution shown in Equation (5.2.2):

$$(v', \eta', b') = (\tilde{v}, \tilde{\eta}, \tilde{b})\exp(i(\alpha x + \beta z - \omega t)) \tag{5.2.2}$$

where α and β are the real input wavenumbers in the streamwise and spanwise directions and $\omega = \omega_r + i\omega_i$ is the complex frequency. The real part of ω is the oscillation frequency of the eigenmode and the imaginary part is the growth rate. ω_i is the significant variable that we are interested in. It determines the local stability of the perturbed state. $(\tilde{v}, \tilde{\eta}, \tilde{b})$ are the eigenfunctions that give us the perturbed state variable shapes and ω_i are the eigenspectra.

With our normal mode solution we can then substitute out the partial derivatives in our velocity, vorticity and density forms to assemble our final eigenvalue system. These substitutions are shown below:

$$\frac{\partial}{\partial t} = -i\omega, \quad \frac{\partial}{\partial x} = i\alpha, \quad \frac{\partial}{\partial y} = \mathcal{D}, \quad \frac{\partial}{\partial z} = i\beta; \quad \frac{\partial^2}{\partial x^2} = -\alpha^2, \quad \frac{\partial^2}{\partial y^2} = \mathcal{D}^2, \quad \frac{\partial^2}{\partial z^2} = -\beta^2$$

As in commonly implemented in HSA, the constant $k^2 = \alpha^2 + \beta^2$ can be introduced. This allows the Laplace operator to be represented as $\nabla^2 = \Delta = \left(\frac{\partial^2}{\partial x^2} + \frac{\partial^2}{\partial y^2} + \frac{\partial^2}{\partial z^2}\right) = \left(\mathcal{D}^2 - k^2\right)$.

5.3 Velocity Form

We are interested in finding a time derivative for the streamnormal velocity perturbation, v', as a function of the reduced state variables, $f(\frac{\partial v'}{\partial t}, v', \eta', b') = 0$, which is the velocity form of the system. We wish to remove the influence of the streamwise and spanwise velocity components. In order to find the velocity form, one most follow the preceding manipulation; $\frac{\partial}{\partial x}$(5.1.9a), $\frac{\partial}{\partial y}$(5.1.9b), $\frac{\partial}{\partial z}$(5.1.9c) to the linearised momentum equations. The outcome is presented below:

$$\frac{\partial}{\partial t}\left(\frac{\partial u'}{\partial x}\right) + \frac{\partial}{\partial x}\left(U\frac{\partial u'}{\partial x}\right) + \frac{\partial}{\partial x}\left(v'\frac{dU}{dy}\right) = -\frac{\partial^2 p'}{\partial x^2} + \frac{1}{Re}\frac{\partial}{\partial x}\left(\nabla^2 u'\right) \tag{5.3.1a}$$

$$\frac{\partial}{\partial t}\left(\frac{\partial v'}{\partial y}\right) + \frac{\partial}{\partial y}\left(U\frac{\partial v'}{\partial x}\right) = -\frac{\partial^2 p'}{\partial y^2} + \frac{1}{Re}\frac{\partial}{\partial y}\left(\nabla^2 v'\right) - \frac{1}{F_h^2}\frac{\partial b'}{\partial y}\cos\theta \tag{5.3.1b}$$

$$\frac{\partial}{\partial t}\left(\frac{\partial w'}{\partial z}\right) + \frac{\partial}{\partial z}\left(U\frac{\partial w'}{\partial x}\right) = -\frac{\partial^2 p'}{\partial z^2} + \frac{1}{Re}\frac{\partial}{\partial z}\left(\nabla^2 w'\right) + \frac{1}{F_h^2}\frac{\partial b'}{\partial z}\sin\theta \tag{5.3.1c}$$

Next we sum Equations (5.3.1a), (5.3.1b) and (5.3.1c) and applying the linearised continuity, Equation (5.1.10), we find:

$$\begin{aligned}
&\frac{\partial}{\partial t}\left(\cancel{\frac{\partial u'}{\partial x}} + \cancel{\frac{\partial v'}{\partial y}} + \cancel{\frac{\partial w'}{\partial z}}\right) + U\frac{\partial}{\partial x}\left(\cancel{\frac{\partial u'}{\partial x}} + \cancel{\frac{\partial v'}{\partial y}} + \cancel{\frac{\partial w'}{\partial z}}\right) + 2\frac{dU}{dy}\frac{\partial v'}{\partial x} \\
&= -\nabla^2 p' + \frac{1}{Re}\left(\frac{\partial^2}{\partial x^2}\left(\cancel{\frac{\partial u'}{\partial x}} + \cancel{\frac{\partial v'}{\partial y}} + \cancel{\frac{\partial w'}{\partial z}}\right) + \frac{\partial^2}{\partial y^2}\left(\cancel{\frac{\partial u'}{\partial x}} + \cancel{\frac{\partial v'}{\partial y}} + \cancel{\frac{\partial w'}{\partial z}}\right) + \frac{\partial^2}{\partial z^2}\left(\cancel{\frac{\partial u'}{\partial x}} + \cancel{\frac{\partial v'}{\partial y}} + \cancel{\frac{\partial w'}{\partial z}}\right)\right) \\
&+ \frac{1}{F_h^2}\frac{\partial b'}{\partial z}\sin\theta - \frac{1}{F_h^2}\frac{\partial b'}{\partial y}\cos\theta
\end{aligned} \tag{5.3.2}$$

This leaves us with the stratified form of the Poisson equation for pressure, shown in Equation (5.3.3) below.

$$\nabla^2 p' = -2\frac{dU}{dy}\frac{\partial v'}{\partial x} + \frac{1}{F_h^2}\frac{\partial b'}{\partial z}\sin\theta - \frac{1}{F_h^2}\frac{\partial b'}{\partial y}\cos\theta \tag{5.3.3}$$

Now, we wish to eliminate the pressure term. By just looking at Equation (5.1.9b) and the stratified Poisson equation for pressure, we can ∇^2(5.1.9b) and $\frac{\partial}{\partial y}$(5.3.3), which gives us:

$$\nabla^2\left(\frac{\partial v'}{\partial t} + U\frac{\partial v'}{\partial x}\right) = -\frac{\partial}{\partial y}\nabla^2 p' + \frac{1}{Re}\nabla^4 v' - \frac{1}{F_h^2}\nabla^2 b'\cos\theta \tag{5.3.4a}$$

$$-\frac{\partial}{\partial y}\nabla^2 p' = 2\frac{\partial}{\partial y}\left(\frac{dU}{dy}\frac{\partial v'}{\partial x}\right) - \frac{1}{F_h^2}\frac{\partial^2 b'}{\partial y \partial z}\sin\theta + \frac{1}{F_h^2}\frac{\partial^2 b'}{\partial y^2}\cos\theta \tag{5.3.4b}$$

Equating the pressure terms together:

$$\nabla^2\left(\frac{\partial v'}{\partial t} + U\frac{\partial v'}{\partial x}\right) - \frac{1}{Re}\nabla^4 v' + \frac{1}{F_h^2}\nabla^2 b'\cos\theta = 2\frac{\partial}{\partial y}\left(\frac{dU}{dy}\frac{\partial v'}{\partial x}\right) - \frac{1}{F_h^2}\frac{\partial^2 b'}{\partial y \partial z}\sin\theta + \frac{1}{F_h^2}\frac{\partial^2 b'}{\partial y^2}\cos\theta \tag{5.3.5}$$

Now looking at second term in Equation (5.3.5), we can simplify it to:

$$\nabla^2\left(U\frac{\partial v'}{\partial x}\right) = U\frac{\partial}{\partial x}\left(\nabla^2 v'\right) + \frac{d^2U}{dy^2}\frac{\partial v'}{\partial x} + 2\frac{dU}{dy}\frac{\partial^2 v'}{\partial x \partial y} \tag{5.3.6}$$

Finally putting Equation (5.3.6) back into Equation (5.3.5) and rearranging we come to the final velocity form:

$$\left[\left(\frac{\partial}{\partial t} + U\frac{\partial}{\partial x}\right)\nabla^2 - \frac{d^2U}{dy^2}\frac{\partial}{\partial x} - \frac{1}{Re}\nabla^4\right]v' + \left[\frac{1}{F_h^2}\left(\nabla^2\cos\theta - \frac{\partial^2}{\partial y^2}\cos\theta + \frac{\partial^2}{\partial y \partial z}\sin\theta\right)\right]b' = 0 \tag{5.3.7}$$

Looking closely at Equation (5.3.7), one can notice that is the stratified form of the Orr-Sommerfeld equation, where the first term is the famous system and the second is the buoyancy contribution.

5.4 Vorticity Form

Next we are interested in finding a time derivative for the wall-normal vorticity perturbation, η', as a function of the reduced state variables, $f(\frac{\partial \eta'}{\partial t}, v', \eta', b') = 0$, which is the vorticity form of the system. Once again we look to manipulate the momentum equations by $\frac{\partial}{\partial x}$(5.1.9c) and $\frac{\partial}{\partial z}$(5.1.9a).

$$\frac{\partial}{\partial t}\left(\frac{\partial u'}{\partial z}\right) + U\frac{\partial^2 u'}{\partial x \partial z} + \frac{dU}{dy}\frac{\partial v'}{\partial z} = -\frac{\partial^2 p'}{\partial x \partial z} + \frac{1}{Re}\frac{\partial}{\partial z}\left(\nabla^2 u'\right) \tag{5.4.1a}$$

$$\frac{\partial}{\partial t}\left(\frac{\partial w'}{\partial x}\right) + U\frac{\partial^2 w'}{\partial x^2} = -\frac{\partial^2 p'}{\partial x \partial z} + \frac{1}{Re}\frac{\partial}{\partial x}\left(\nabla^2 w'\right) + \frac{1}{F_h^2}\frac{\partial b'}{\partial x}\sin\theta \tag{5.4.1b}$$

Finally subtracting Equation (5.4.1b) from Equation (5.4.1a) and substituting $\eta' = \left(\frac{\partial u'}{\partial z} - \frac{\partial w'}{\partial x}\right)$ will give us the stratified Squire system:

$$\left[\frac{\partial}{\partial t} + U\frac{\partial}{\partial x} - \frac{1}{Re}\nabla^2\right]\eta' + \left[\frac{dU}{dy}\frac{\partial}{\partial z}\right]v' + \left[\frac{1}{F_h^2}\frac{\partial}{\partial x}\sin\theta\right]b' = 0 \tag{5.4.2}$$

Equation (5.4.2) is the vorticity form of our final system of equations. The first two terms is the famous Squire equation plus the added last term, which is the stratification contribution.

5.5 Density Transport Form

Finally we are interested in finding the last time derivative equation of the final stratified system for the dimensionless buoyancy perturbation, b', as a function of the reduced state variables, $f(\frac{\partial b'}{\partial t}, v', \eta', b') = 0$, which is the density transport form of the system. Subbing in that $Y = y\cos\theta - z\sin\theta$, the linearised density transport gives:

$$\left[\frac{\partial}{\partial t} + U\frac{\partial}{\partial x} - \frac{1}{ReSc}\nabla^2\right]b' - \left[\frac{\cos\theta}{F_h^2}\right]v' + \left[\frac{\sin\theta}{F_h^2}\right]w' = 0 \tag{5.5.1}$$

5.6 Final Equations

Before we sub in the normal-mode solution derivative substitutions, notice how Equation (5.5.1) has a $\tilde{w}$ term, which is not one of the reduced state variables, and is incorporated in the wall-normal voriticity. So to remove this term, we carry out the analysis described below.

5.6.1 $\tilde{w} = f(\tilde{v}, \tilde{\eta})$

Our wall-normal vorticity can be written in normal-mode form:

$$\tilde{\eta} = (\frac{\partial \tilde{u}}{\partial z} - \frac{\partial \tilde{w}}{\partial x}) = i\beta\tilde{u} - i\alpha\tilde{w} \tag{5.6.1}$$

We can also do the same with the linearised continuity equation:

$$i\alpha\tilde{u} + \mathcal{D}\tilde{v} + i\beta\tilde{w} = 0 \tag{5.6.2}$$

We can rearrange the continity equation in terms of $\tilde{u} = \frac{i}{\alpha}(\mathcal{D}\tilde{v} + i\beta\tilde{w})$. Subbing this into Equation (5.6.1), we find $\tilde{w} = f(\tilde{v}, \tilde{\eta})$:

$$\tilde{w} = \frac{1}{k^2}\big(i\beta\mathcal{D}\tilde{v} + i\alpha\tilde{\eta}\big) \tag{5.6.3}$$

Finally substitute in normal mode solution into Equations (5.3.7), (5.4.2) and (5.5.1), while also subbing in Equation (5.6.3) into Equation (5.5.1), to give the three main system of equations we wish to solve:

$$\big[(-i\omega + i\alpha U)(k^2 - \mathcal{D}^2) + i\alpha\mathcal{D}^2U + \frac{1}{Re}(k^2 - \mathcal{D}^2)^2\big]\tilde{v} + \big[\frac{1}{F_h^2}\big(k^2\cos\theta - i\beta\mathcal{D}\sin\theta\big)\big]\tilde{b} = 0 \tag{5.6.4a}$$

$$\big[(-i\omega + i\alpha U) + \frac{1}{Re}(k^2 - \mathcal{D}^2)\big]\tilde{\eta} + \big[i\beta\mathcal{D}U\big]\tilde{v} + \big[\frac{1}{F_h^2}i\alpha\sin\theta\big]\tilde{b} = 0 \tag{5.6.4b}$$

$$\big[(-i\omega + i\alpha U) + \frac{1}{ReSc}(k^2 - \mathcal{D}^2)\big]\tilde{b} + \left[\left(\frac{\sin\theta}{F_h^2k^2}\right)i\beta\mathcal{D} - \left(\frac{\cos\theta}{F_h^2}\right)\right]\tilde{v} + \left[\left(\frac{\sin\theta}{F_h^2k^2}\right)i\alpha\right]\tilde{\eta} = 0 \tag{5.6.4c}$$

5.6.2 Matrix System

It would be convenient to put our system of equations into matrix form to give our final eigenvalue problem. Equations (**??**) and (5.6.4b) in matrix form yields:

$$-i\omega\begin{pmatrix}(k^2-\mathcal{D}^2) & 0 & 0\\ 0 & 1 & 0\\ 0 & 0 & 1\end{pmatrix}\begin{pmatrix}\tilde{v}\\ \tilde{\eta}\\ \tilde{b}\end{pmatrix} + \begin{pmatrix}\mathcal{L}_{OS} & 0 & \mathcal{L}^b_{OS}\\ i\beta\mathcal{D}U & \mathcal{L}_{SQ} & \frac{1}{F_h^2}i\alpha\sin\theta\\ \mathcal{L}_v & (\frac{\sin\theta}{F_h^2k^2})i\alpha & \mathcal{L}_b\end{pmatrix}\begin{pmatrix}\tilde{v}\\ \tilde{\eta}\\ \tilde{b}\end{pmatrix} = \mathbf{0} \tag{5.6.5}$$

In a more compact form:

$$\mathbf{L}\tilde{\mathbf{q}} = i\omega\mathbf{M}\tilde{\mathbf{q}} \tag{5.6.6}$$

where:

$$\tilde{\mathbf{q}} = \begin{pmatrix} \tilde{v} \\ \tilde{\eta} \\ \tilde{b} \end{pmatrix} \quad \mathbf{L} = \begin{pmatrix} \mathcal{L}_{OS} & 0 & \mathcal{L}^b_{OS} \\ i\beta\mathcal{D}U & \mathcal{L}_{SQ} & \frac{1}{F_h^2} i\alpha \sin\theta \\ \mathcal{L}_v & \left(\frac{\sin\theta}{F_h^2 k^2}\right) i\alpha & \mathcal{L}_b \end{pmatrix} \quad \mathbf{M} = -i\omega \begin{pmatrix} (k^2 - \mathcal{D}^2) & 0 & 0 \\ 0 & 1 & 0 \\ 0 & 0 & 1 \end{pmatrix}$$

$$\mathcal{L}_{OS} = i\alpha U(k^2 - \mathcal{D}^2) + i\alpha\mathcal{D}^2 U + \frac{1}{Re}(k^2 - \mathcal{D}^2)^2 \tag{5.6.7a}$$

$$\mathcal{L}^b_{OS} = \frac{1}{F_h^2}\left(k^2 \cos\theta - i\beta\mathcal{D}\sin\theta\right) \tag{5.6.7b}$$

$$\mathcal{L}_{SQ} = i\alpha U + \frac{1}{Re}(k^2 - \mathcal{D}^2) \tag{5.6.7c}$$

$$\mathcal{L}_v = \left(\frac{\sin\theta}{F_h^2 k^2}\right) i\beta\mathcal{D} - \left(\frac{\cos\theta}{F_h^2}\right) \tag{5.6.7d}$$

$$\mathcal{L}_b = i\alpha U + \frac{1}{ReSc}(k^2 - \mathcal{D}^2) \tag{5.6.7e}$$

Note that terms $\mathcal{L}_{OS}$ is the famous Orr-Sommerfeld coefficient and the buoyancy contribution is represented by $\mathcal{L}^b_{OS}$. Notice that its influence on the Orr-Sommerfeld system reduces with increasing F_h (as stratification strength reduces). $\mathcal{L}_{SQ}$ is the Squire coefficient and its buoyancy contribution is through the term $\frac{1}{F_h^2} i\alpha\sin\theta$. Like the Orr-Sommerfeld system, the stratification influence is reduced with increasing F_h. The matrix system and compact form is following the same nomenclature as REFERENCE page 60 of Schmid and Henningson. The idea was to build on the Orr-Sommerfeld/Squire system solved there. In the limit of $F_h \to \infty$, the matrix system (5.6.5) reduces to the original equations.

5.7 Boundary Conditions

We seek to find conditions at the boundary for our main state variables $(\mathbf{u}', \eta', p', b')$ and hence our reduced state space (v', η', b'). Firstly, looking at the velocity perturbations, $\mathbf{u}'$, the main boundary conditions are imposed from the certain approximations and assumptions that we make. The core assumption of no-slop conditions at the boundaries of the shear plane gives the conditions:

$$u' = 0 \tag{5.7.1a}$$

$$w' = 0 \tag{5.7.1b}$$

Furthermore, we can exploit these conditions along with the fully developed shear velocity profile to the linearised incompressible continuity equation to give us the condition:

$$\cancel{\frac{\partial u'}{\partial x}} + \frac{\partial v'}{\partial y} + \cancel{\frac{\partial w'}{\partial z}} = 0 \tag{5.7.2a}$$

$$\mathcal{D}v' = 0 \tag{5.7.2b}$$

Next we can employ the non-impenetrable wall assumption. This assumptions implies that the walls at the boundaries of the shear plane will not leak flow, hence velocity perturbations here must be zero, thus this develops the boundary condition:

$$v' = 0 \tag{5.7.3}$$

For the pressure perturbation, Dirichlet conditions is normally implemented. As for the buoyancy perturbation, a range of boundary conditions could be used. PAPER 2 imposes the no-flux conditions at the walls, hence has conditions $\mathcal{D}b' = 0$, whereas PAPER 5 sets buoyancy perturbations to zero at the walls.

In discussion, PAPER 2 reiterates how the density wall conditions were chosen to satisfy no-flux by imposing Neumann conditions. They carried out a test case (results were not presented), that suggested applying an insulating wall condition yields very similar results, suggesting a certain robustness in the implemented scheme. For simplicity a Dirichlet buoyancy condition is employed along with the wall-normal voriticity perturbation:

$$b' = 0 \tag{5.7.4a}$$
$$\eta' = 0 \tag{5.7.4b}$$

So in conclusion, we impose Dirichlet boundary conditions $(v', \eta', b') = \mathbf{0}$. Our fundamental eigenvalue problem is therefore solved by inputting wavenumbers (α, β) and outputting the eigenvalue $i\omega$. Our fundamental parameters to examine the shear flow stability is the dimensionless parameters Re and F_h, while also changing the tilt angle θ. The value of Schmidt number that is commonly used is $Sc = 700$, hence this value was taken constant. Analysis on the influence of Sc will be presented later.

Chapter 6

Numerical Framework

The fundamental eigenvalue system to be solved is given in Section 5.6.5. This system was to be computed numerically by discretising the equations from a PDE into a matrix operation numerical scheme. The famous scheme that is typically employed is the Chebyshev Transform Method. After that, the solver would be embedded into an algorithm to sort the eigenspectra in order of growth rate with growing stability. Building on top of the algorihm one can generate data like a neutral stability curve and other methods to visualise the eigenspectra and eigenfunctions.

In this Chapter we look to introduce the MATLAB Solver that implements the numerical solver for the system. We will first discuss the code's main architecture and to improve the scripts usability, it was written as a function to optimise its flexibility in many contexts. This requires an overview of the main functions architecture and a discussion of the useful sub-functions that were implemented and before the script could be used to investigate our area of interest, it must be validated against existing works.

6.1 Numerical Method

As aforementioned, the implemented numerical scheme was the Chebyshev Transform Method. It transforms a generic continuous function $u(x)$ into discrete points. More of this will be discussed later but first we must introduce the function architecture.

6.1.1 OS_SQ_Stratified_Solver.m

The main function is named OS_SQ_Stratified_Solver.m, which solves the linear stability problem for a stratified Orr-Sommerfeld/Squire system. Generally, the Solver follows the same routine as many scripts with an input, initialisation, solver, post-processing and visualisation. The input parameters are set by the user in the command window. These inputs are firstly validated through a sub-function named 'inputValidation.m'. This function ensures that the inputs are of an appropriate data type and value which maximises ease of functionality for the user. Once the inputs are validated, the Solver computes the eigenspectra and outputs three main variables; the unsorted eigenspectra, ω. This allows the user to investigate the separate branches. The other main outputs include the eigenfunctions of the most unstable eigenmode. This allows the user to produce plots of the perturbation shape of the most unstable growth rate allowing investigation of the stability mechanisms. Finally, the function outputs the ordered eigenspectra, in terms of decreasing instability of the growth rate, ω_i. This is carried out using the sub-function 'eigenSort.m'.

The main inputs to the Solver are $(flow, N, \alpha, \beta, Re, F_h, \theta)$, where $flow$ is the chosen shear base flow (either pCf or pPf), N is the number of Chebyshev grid points, which shall be discussed later, and the rest are the

main flow properties that will be studied on their effect to linear stratified stability.

Give the option to visualise the e/spectra and e/functions with another input. Function can then be run multiple times to produce plots. Add figure showing command window output. Subsection of each function MATLAB.

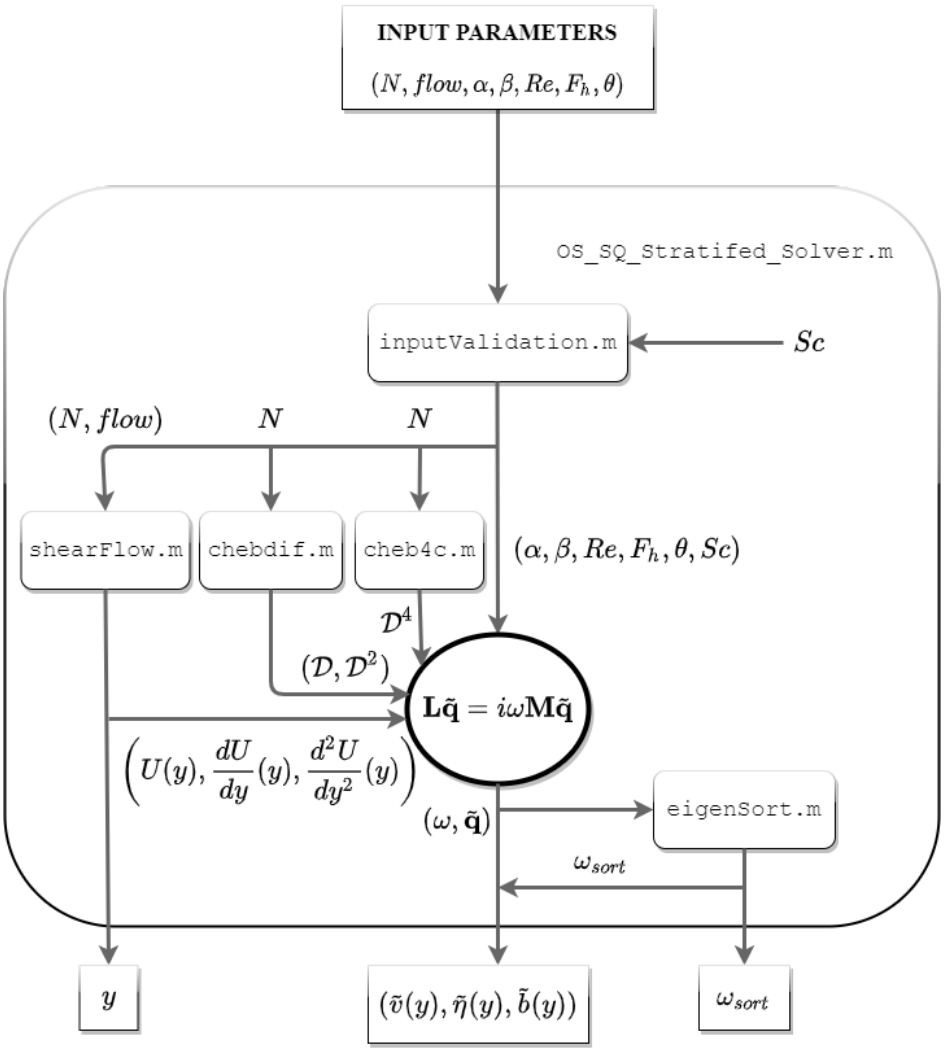

Figure 6.1: Main solver infrastructure 'OS_SQ_Stratified_Solver.m'.

6.1.2 Chebyshev Transform

The Chebyshev Transform is a type of Discrete Transform Method. They can be viewed as semi-analytical alternatives to finite differences for spatial differentiation applications where high degrees of accuracy are required. These transform methods produce solutions to partial differential equations. A classic type of Discrete Transform Method is the Fourier Series. However, this is not appropriate for representing non-periodic functions, the convergence of the series with increasing number of terms is rather slow. The Chebyshev polynomial expansion is useful for non-periodic data.

An arbitrary smooth function can be represented in terms of a series of orthogonal polynomials, which are the eigenfunctions. An advantage of using polynomial expansions to approximate arbitrary functions is their superior resolution capabilities near boundaries. We shall be implementing the the Chebyshev polynomial class. Our arbitrary smooth function, $u(x)$, defined in the domain $-1 \leq x \leq 1$, is approximated by the finite series of Chebyshev polynomials:

$$u(x) = \sum_{n=0}^{N} a_n T_n(x), \tag{6.1.1}$$

where n represents the polynomial order, N is the finite highest order polynomial and a_n are the Chebshev coefficients with $T_n(x)$ representing the Chebyshev polynomals of order n.

The Chebyshev polynomials are solutions of the differential eigenvalue problem:

$$\frac{d}{dx}\left(\sqrt{1-x^2}\frac{dT_n}{dx} + \frac{\lambda_n}{\sqrt{1-x^2}}T_n\right) = 0 \tag{6.1.2}$$

where $\lambda_n = n^2$ are the eigenvalues. The first few Chebyshev polynomials are $T_0 = 1$, $T_1 = x$, $T_2 = 2x^2 - 1$ and so on. A key property of the Chebyshev polynomials is that they become simple cosines with the transformation of the independent variable $x = \cos\theta$, which maps $1 \leq x \leq 1$ into $0 \leq \theta \leq \pi$. The transformation is:

$$T_n(\cos\theta) = \cos n\theta. \tag{6.1.3}$$

This is a useful feature of Chebyshev polynomial expansions as the representation is reverted to cosine transforms and in the discrete case one can take advantage of the First Fourier Transform algorithm. Exploiting trigonometry, the following recursive relation can be used to generate $T_n(x)$:

$$T_{n+1}(x) + T_{n-1}(x) = 2xT_n(x) \qquad b \leq 1. \tag{6.1.4}$$

Other important properties of Chebyshev polynomials are listed below:

- $|T_n(x)| \leq 1$ in domain $-1 \leq x \leq 1$
- $T_n(\pm 1) = (\pm 1)^n$.

For numerical analysis, the domain is discretised using a cosine mesh:

$$x_j = \cos\frac{\pi j}{N} \qquad j = N, N-1, ..., 1, 0. \tag{6.1.5}$$

The discrete Chebyshev transform representation of u on a discrete set of points is defined as:

$$u_j = \sum_{n=0}^{N} a_n T_n(x) = \sum_{n=0}^{N} a_n \cos\frac{n\pi j}{N} \qquad j = 0, 1, 2, ..., N \tag{6.1.6}$$

Note that our smooth functions are the state variables $(\tilde{v}(y), \tilde{\eta}(y), \tilde{b}(y))$ for the domain $-1 \leq y \leq 1$:

$$\tilde{v}_j = \sum_{n=0}^{N} a_n T_n(y) = \sum_{n=0}^{N} a_n \cos\frac{n\pi j}{N} \tag{6.1.7a}$$

$$\tilde{\eta}_j = \sum_{n=0}^{N} a_n T_n(y) = \sum_{n=0}^{N} a_n \cos\frac{n\pi j}{N} \tag{6.1.7b}$$

$$\tilde{b}_j = \sum_{n=0}^{N} a_n T_n(y) = \sum_{n=0}^{N} a_n \cos\frac{n\pi j}{N} \tag{6.1.7c}$$

The next step is to develop the relationship between the Chebyshev coefficients of the function and its derivatives:

$$u'(x) = \sum_{n=0}^{N-1} b_n T_n(x) \tag{6.1.8}$$

where b_n are the derivative coefficients and note that the derivative polynomial is of order $N-1$. We can differentiate Equation (6.1.1) and equate it to Equation (6.1.8). After some manipulation as shown in APPENDIX, the relation between a_n and b_n can be found from:

$$c_{n-1}b_{n-1} - b_{n+1} = 2na_n \qquad n = 1, 2, ..., N \tag{6.1.9}$$

where $b_N = b_{N+1} = 0$. In summary to compute the derivative of a function u, firstly compute its Chebyshev coefficients using APPENDIX, then the derivative coefficients can be obtained from Equation (6.1.9). The derivative function can then be represented by Equation (6.1.8). As a final comment we can express the Chebyshev derivatives in matrix form and this was what was implemented in the code. Hence all derivatives in the y-direction, $\mathcal{D}, \mathcal{D}^2$ and $\mathcal{D}^4$ were approximated by a matrix of Chebyshev coefficients.

APPENDIX THE CHEBYSHEV COEFFICIENTS APPENDIX PROOF OF Bn TO An

6.1.3 Chebyshev Grid Point Convergence

In terms of computational cost, it is advantages to minimise the number of Chebyshev grid points used, N. However, using too few grid points would reduce the accuracy of the Chebyshev representation of the smooth function. Therefore, it is useful to carry out a grid point convergence study to evaluate the variation of the solutions as N is increased. The outputted growth rate, ω_i, was examined and plotted against N for both shear flows; pCf and pPf. The analysis allowed us to determine the required number of grid points until the results convergence; the results do not change from a further increase in N.

The convergence plots can be observed in Figure 6.2 and 6.3, which represents the study carried out for the pCf and pPf respectively. For the convergence study, Re and F_h were held constant at values of 1000 and 1, as their value has no significance on convergence. Figures 6.2(a) and 6.3(a) represent the convergence of the growth rate with N for the cases with the tilt angle, θ, being 30 and 60 degrees. Likewise, Figures 6.2(b) and 6.3(b) represent the convergence of the growth rate for the cases with different combinations of wavenumbers.

One should observe how the input parameters have no influence in the convergence of the solution as all the curves appear to converge at the similar points. All the curves illustrate the same features, they convergence at $N \approx 100$ and then begine to diverge once again at $N \geq 200$. The latter suggests the

existence of Gibbs phenomenon where the solution typically divergences at large mesh densities. Therefore, an appropriate value for N would be within the range: $100 \leq N \leq 200$. To minimise computation cost and reinforced by other works, the number of grid points for all simulations was at a value of: $N = 100$.

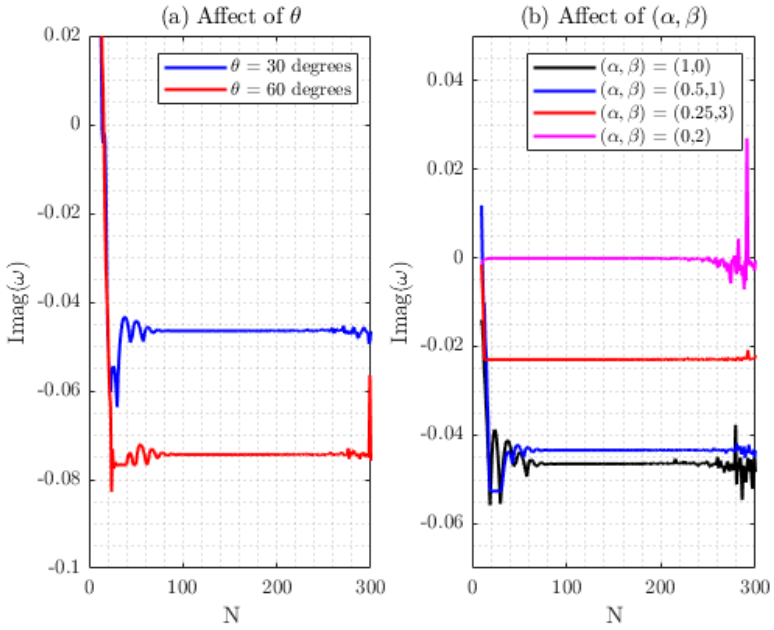

Figure 6.2: Convergence of ω_i with varying N for the pCf base profile, where (a) represents different tilt angles and (b) has a variety of wavenumbers.

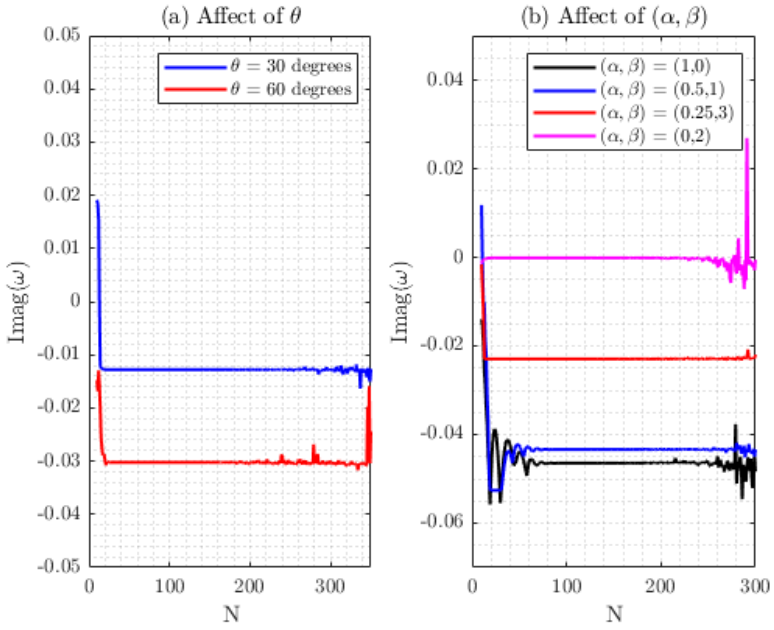

Figure 6.3: Convergence of ω_i with varying N for the pPf base profile, where (a) represents different tilt angles and (b) has a variety of wavenumbers.

6.2 Implementing Boundary Conditions

As discussed, Dirichlet boundary conditions for each state variable were implemented: $(\tilde{v}, \tilde{\eta}, \tilde{b}) = \mathbf{0}$. These conditions could be intuitively imposed by removing the outer bracket of the resulting Chebyshev matrices by removing the first and last rows and columns. This would create spurious modes, hence a more elegant method was proposed by embedding the clamped condition right within the fourth order Chebyshev differential matrices. REFERENCE provides the MATLAB function 'cheb4c.m' which generates the fourth order Chebyshev differential matrices with the clamped conditions embed, while 'chebdiff.m' generates the Chebyshev differential matrices of the first three orders.

6.3 Validation Approach

The solver was designed to maximise resuablity and flexibility for further work thus it was important to ensure the script could be built on for other systems and base flows. To achieve this, the solver must firstly be validated against existing research. Data was used from multiple sources including REFERENCES. It is important that as many aspects of the script was validated. It is important to notice that there are slight discrepancies between the approaches taken to reach the final eigenvalue problem. For example, Facchini does not use the Orr-Sommerfeld governing equations. Adding shear flows to the solver is simply done through adding the velocity profiles in the 'shearFlow.m' function, while ensuring the new base flow has a tag when called by the shear flow input.

6.3.1 Unstratified Case

The solver was firstly developed from a Orr-Sommerfeld/Squire system with an unstratified pCf and pPf flow. This allowed direct validation with the Schmid and Henningson, which contains data of the most unstable eigenmodes of the pCf and pPf under defined conditions.

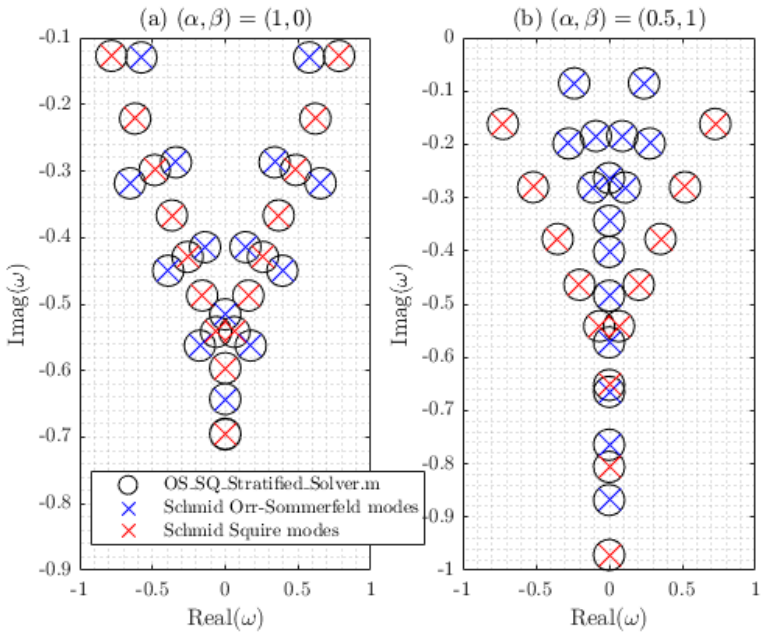

Figure 6.4: Comparison of the eigenspectra on the ω complex plane for different wavenumbers with the pCf.

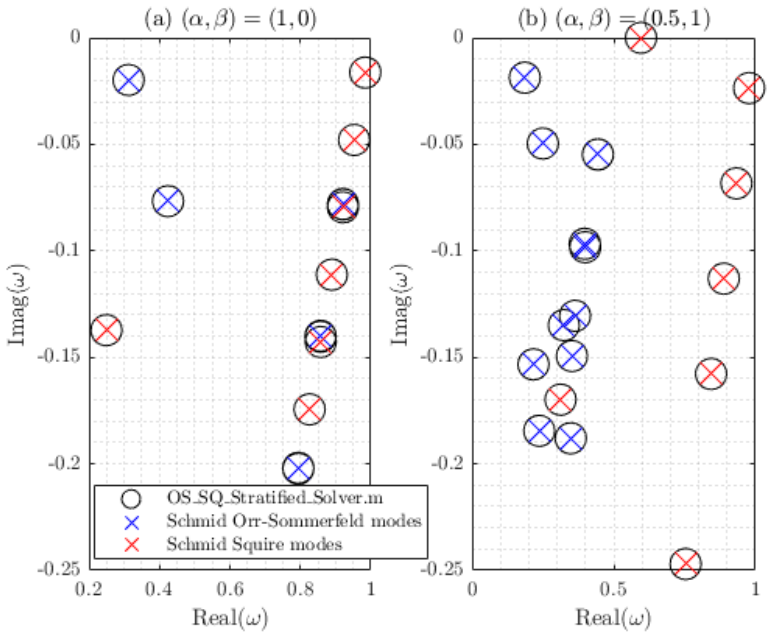

Figure 6.5: Comparison of the eigenspectra on the ω complex plane for different wavenumbers with the pPf.

Figure 6.4 shows the data points of the eigenspectra from state variables $(\tilde{v}, \tilde{\eta})$ for the pCf. The inputs were Re of 800 and the wavenumbers, (α, β), were $(1, 0)$ and $(0.5, 1)$ for Figures 6.4(a) and (b) respectively. One can note how the eigenvalues match exactly with the Schmid Orr-Somerfeld and Squire modes. Similarly, Figure 6.5 shows the eigenspectra for the pPf, with a Re of 2000 but with the same wavenumbers as the pCf case. Again the eigenvalues from my unstratified solver matched Schmid's results exactly.

Further validation was carried out for the unstratified case using the pPf. A famous result is that the transition Re for $(\alpha, \beta) = (1, 0)$ is 5772 which the solver outputs REFERENCE. Likewise, for input parameters $(\alpha, \beta, Re) = (1, 0, 10000)$, the most unstable eigenmode has value $0.2375 + 0.0037i$. These results proved that the developed unstratified solver was working as expected and now the stratification was simply needed to be implemented. To the end, the state varable $\tilde{b}$ needed to be added to the system. The new system needed to converge to the unstratified case as $F_h \infty$, as this represents a negligible stratification strength.

6.3.2 Stratified Case

Facchini carried out LSA on a pCf with spanwise stratification. One of Facchini's main results was that one stationary growing mode appears at $(\alpha, \beta, Re, F_h) \approx (0.8, 5, 1000, 1)$. This produced ω with $\omega_r = 0$ and $\omega_i > 0$. Inputting these variables into the solver 'OS_SQ_Stratified_Solver.m', with tilt angle at 90 degrees, outputted a single unstable mode with value: 0.0000 + 0.0127i. This matches the findings of Facchini exactly.

Following this result, Facchini produces a plot of the full eigenspectra of the most unstable mode at $Re = 1000$ and $F_h = 1$, with wavenumbers $(0.815, 4.937)$. The plot is shown in Figure 6.6(b), while the result produced from my solver is shown in Figure 6.6(a).

The significant result is the single unstable eigenmode that crosses the ω_i axis. Figure 6.6 magnifies this result through the inset which is the area delimited by the red triangle, expressing the single unstable mode.

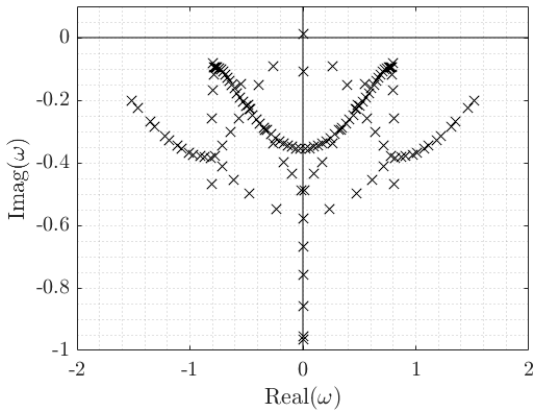

(a) Result from 'OS_SQ_Stratified_Solver.m'.

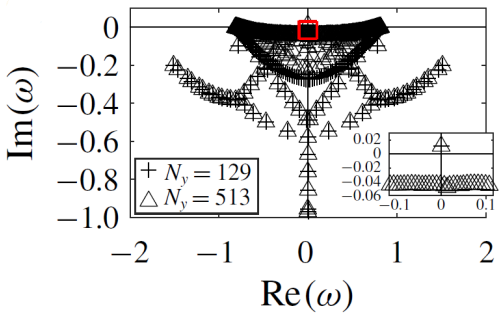

(b) Result from Facchini.

Figure 6.6: Complex plane plot of ω with input parameters $(\alpha, \beta, Re, F_h) = (0.815, 4.937, 1000, 1)$.

The result from my solver matches this result as a lone eigenvalue exists in the upper half plane. Likewise, notice how the shape of the eigenspectra is similar providing further support for the accuracy of the developed solver. There are some differences however which would be important to note. Facchini's result has a much richer eigenspectra given that the state variables implemented were $(\tilde{\mathbf{u}}, \tilde{p}, \tilde{b})$. This reinforces our decision to reduce the state variables to reduce the computational cost. Moreover, Figure 6.6 plots $N = 129$ and 513, whereas my solver uses $N = 100$. Notice how Facchini's result does not appear to exhibit Gibb's phenomenon at $N > 200$ suggesting that the numerical system used is well resolved, however at the expensive of a large computational cost.

Finally, we will validate the outputted eigenfunctions from the solver. Figures 6.7 and 6.8 show the velocity and buoyancy perturbations with input parameters $(\alpha, \beta, Re, F_h) = (0.767, 4.937, 10000, 1)$ with results obtained from my solver and Facchini.

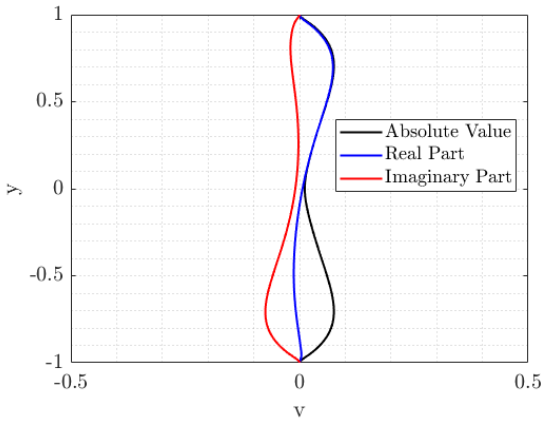

(a) Result from 'OS_SQ_Stratified_Solver.m'.

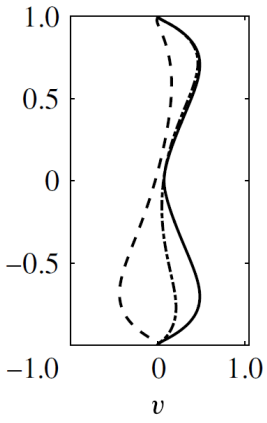

(b) Result from Facchini.

Figure 6.7: Eigenfunctions of the most unstable eigenmode showing the vertical velocity field, where (a) shows my result and (b) from Facchini. Note that in (b) the solid line refers to the absolute value, dashed-dotted line the imaginary part and the dashed line the real part.

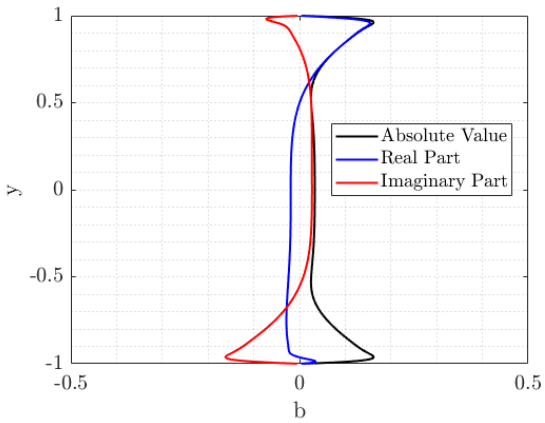

(a) Result from 'OS_SQ_Stratified_Solver.m'.

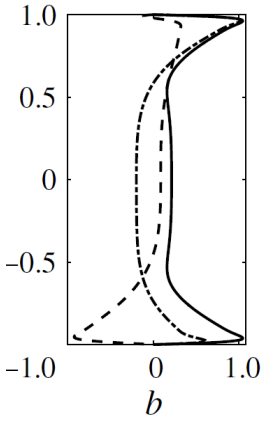

(b) Result from Facchini.

Figure 6.8: Eigenfunctions of the most unstable eigenmode showing the buoyancy perturbation, where (a) shows my result and (b) from Facchini. Note that in (b) the solid line refers to the absolute value, dashed-dotted line the imaginary part and the dashed line the real part.

Note that the wall-normal voriticity perturbation could not be validated as it was not a state variable used by Facchini. Observing each Figure we can see that the shapes of the perturbations matches exactly. There are some discrepancies, which appears from the differences in the systems employed. Also, Facchini normalises the perturbations with the maximum perturbation in the u-field, whereas my solver does not normalise the eigenfunctions.

As a final result, it is useful to check whether the stratified system converges to the original Orr-Sommerfeld/Squire system in the limit of $(Re, Sc) \to \infty$, which is does. This can be easily observed by looking at the system of Equations (5.6.5), where it is clear to observe that all the buoyancy contributions, $\tilde{b} \to 0$ in this limit as the contributions are inversely proportional to F_h.

Chapter 7

Results and Discussion

This chapter will review the main results that were generated from the developed MATLAB Solver; `OS_SQ_Stratified_Solver.m`. The results were found from varying the main inputs, while fixing the Schmid number at 700 (as discussed earlier). Likewise, from the convergence study discussed in the previous section, the number of Chebyshev grid points was fixed to a value of 100. The remaining input parameters that were varied are $(\alpha, \beta, Re, F_h, \theta)$ for a chosen base profile; either pCf or pPf. With these parameters, the most unstable eigenmode was extracted, $\omega_{i,max}$. Likewise, the eigenfunctions of the most unstable eigenmode could be outputted should the user request it.

Given time, a broad range of tilt angles could have been studied to fully investigate the inalignment influences. However, due to time restricts, the main angles that were investigated were 5, 30, 60, 80 degrees, where 5 and 80 degrees were to represent a small and heavy tilt angle. This would give us a strong indication of how the behaviour of the flow evolves from the aligned stratification case to the spanwise case.

The results were categorised into varying certain input parameters while holding the remaining parameters constant. Firstly, the outputted eigenspectra was examined to provide an insight on the features of the complex frequency. Next, the wavenumbers were swept to find the region where instabilities are found. As stated by Deloncle, Chomaz and Billant (2006), two-dimensional instabilities are not expected to dominate, hence reinforcing an interest in three-dimensional turbulence thus non-zero values of (α, β). Next the influence of the tilt angle on the critical Reynolds number, Re_{crit} shall be analysed. Furthering our interest in Re, investigation on the influence of Re on the growth rate is carried out. After that, the F_h effects are examined and finally investigation of the eigenfunctions allow the visualisation of the perturbations providing an idea on the stability mechanisms. Finally, brief comments on the influence of Sc shall be included.

7.1 Eigenspectra

Below plots of the eigenspectra for the pCf and pPf are presented in Figures 7.1 and 7.2 respectively. The input parameters where $(Re, F_h) = (10000, 1)$ for both base flows and the wavenumbers were $(\alpha, \beta) = (0.8, 5)$ for the pCf and $(\alpha, \beta) = (1.5, 6)$ for the pPf. These wavenumbers were chosen as these are the primary regions of instability that appears as the tilt angle increases. This will be made clearer in the neutral stability plots to be presented in Section 7.2. The tilt angle was varied and the subplots in the Figures show the results for $\theta = 5$, 30, 60 and 80 degrees. Both Figures have red points which represents the most unstable eigenmode.

Observing Figure 7.1, one can notice how the eigenspectra has a symmetrical feature with respect to the

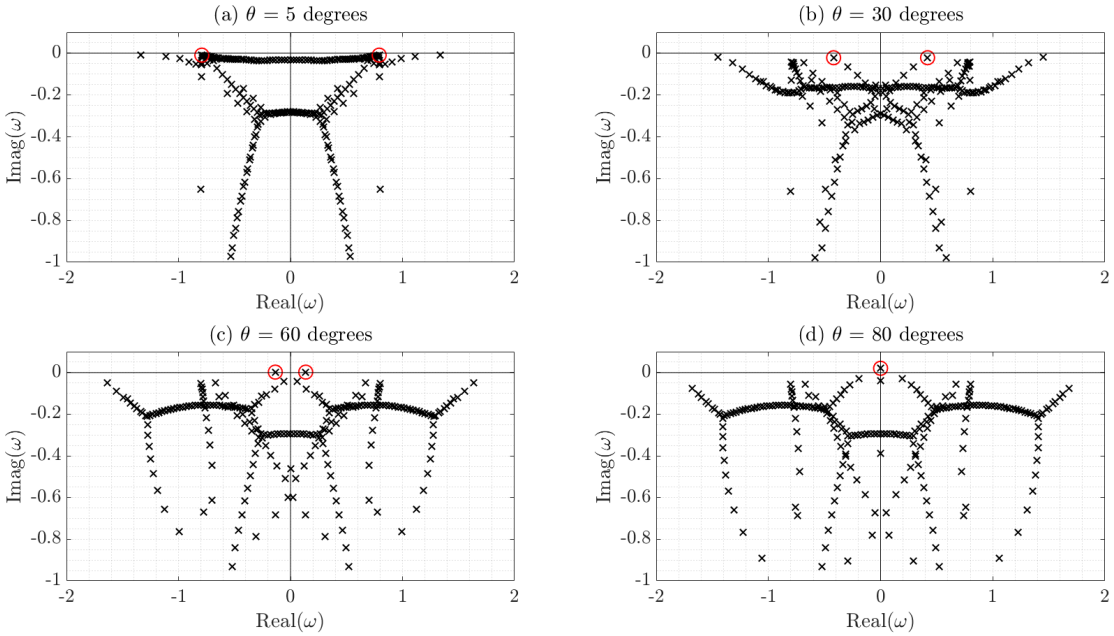

Figure 7.1: Eigenspectra of the pCf base fluid with inputs $(\alpha, \beta, Re, F_h) = (0.8, 5, 10000, 1)$ with subplots of varying tilt angle θ.

real axis, where for a certain growth rate, there is a conjugate pair. One can observe how the eigenmodes break down into various branches as the inalignment is strengthened. This illustrates how the shear and stratification tilt produces more complex flow structures. However, the most significant eigenmode is with most unstable growth rate (highlighted in red). The value of ω_i becomes more positive as the tilt angle is raised. This suggests that the inalignment has a destabilising consequence to the base flow. Notice how as the tilt angle increases, the oscillatory frequency of the most unstable mode (ω_r) decreases in magnitude, as the conjugate pairs move closer together. Between the inalignment angle; 60 degrees and 80 degrees, the most unstable eigenmodes coalesce to produce a single unstable eigenmode with zero oscillatory frequency. Facchini (2018) found the same result, that at 90 degrees, for the critical (Re, F_h), the single unstable mode was non-oscillatory. It is key to note that the instability does not arise at the moment of coalescence, as through observing Figure 7.1(c), the two conjugate eigenmodes are in the upper half plane.

Now looking at Figure 7.2, the symmetry of the eigenvalues does not appear. The eigenspectra is dominated in the lower right plane, with an array of eigenmodes with positive ω_r and stable ω_i. Like the pCf, the most unstable eigenmode becomes more unstable as the tilt angle increases, so the stratification shear inalignment continues to destablise the pPf base flow as well. Moreover, as the tilt angle increases, the eigenspectra splits into multiple branches which also shows the increase in complexity of the perturbations as the tilt angle increases. This displays signs of consistency of the influence of stratification inalignment to the stabililty of shear flows. However, unlike the pCf, there only exists a single unstable mode at all tilt angles.

Note that the symmetrical and assymmetrical features of the eigenspectra, for the pCf and pPf respectively, is also found in the unstratified case with the Orr-Sommerfeld and Squire system, shown in Figures 6.4 and 6.5.

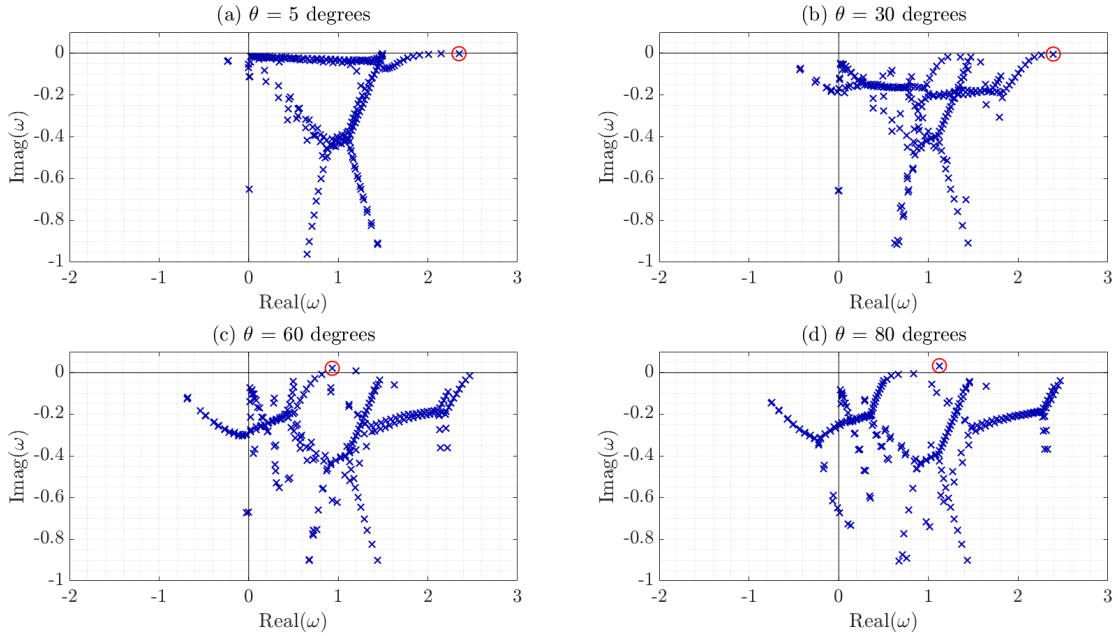

Figure 7.2: Eigenspectra of the pPf base fluid with inputs $(\alpha, \beta, Re, F_h) = (1.5, 6, 10000, 1)$ with subplots of varying tilt angle θ.

7.2 Sweeping Wavenumbers, (α, β)

As a first result, it would be useful to find the region of instability in the wavenumber state space. Therefore, this requires neutral stability plots which are shown in Figures 7.3 to 7.6.

To this end, the stratified solver was run sequentially for a range of wavenumbers while fixing parameters $(Re, F_h, \theta) = (10000, [1, 0.5], [5, 30, 60, 80])$. Figures 7.3 and 7.4 are for the pCf and Figures 7.5 and 7.6 are for the pPf. In these Figures, subplot (a) represents a tilt angle of 60 degrees and (b) with a tilt angle of 80 degrees. Note that results for an inalignment of 5 and 30 degrees has not been shown, as the flow was found to always be stable in these cases. This result is consistent with what was found in the eigenspectra plots of Section 7.1. Notice each of the plots exhibit a red cross. This point represents the most unstable eigenmodes. It is interesting to note that this point is the same for each base flow, which suggests the most unstable point is independent of F_h and θ.

Observing Figure 7.3, the instability bubble is found around the range of wavenumbers $(\alpha, \beta) = ([0.7, 0.8], [4, 5])$. As the tilt angle increases, the instability bubble appears around this region and exhibits slow growth, in the wavenumber plane, which continues until the stratification is aligned spanwise. The area of this instability region is relatively small compared with the pPf cases suggesting that stratified pCf instability is uncommon.

Next, looking at the influence of F_h, by comparing Figures 7.3 and 7.4, increasing the stratification appears to destabilise the flow for a certain tilt angle as the instability region is of a higher area. The increase in the range of instability is small in α, however for β the flow destablises for almost seven times the range when F_h was decreased from 1 to 0.5. To give us a deeper understanding of this finding, further analysis on the influence of F_h to the stability of tilted stratifed shear will be included in Section 7.4.

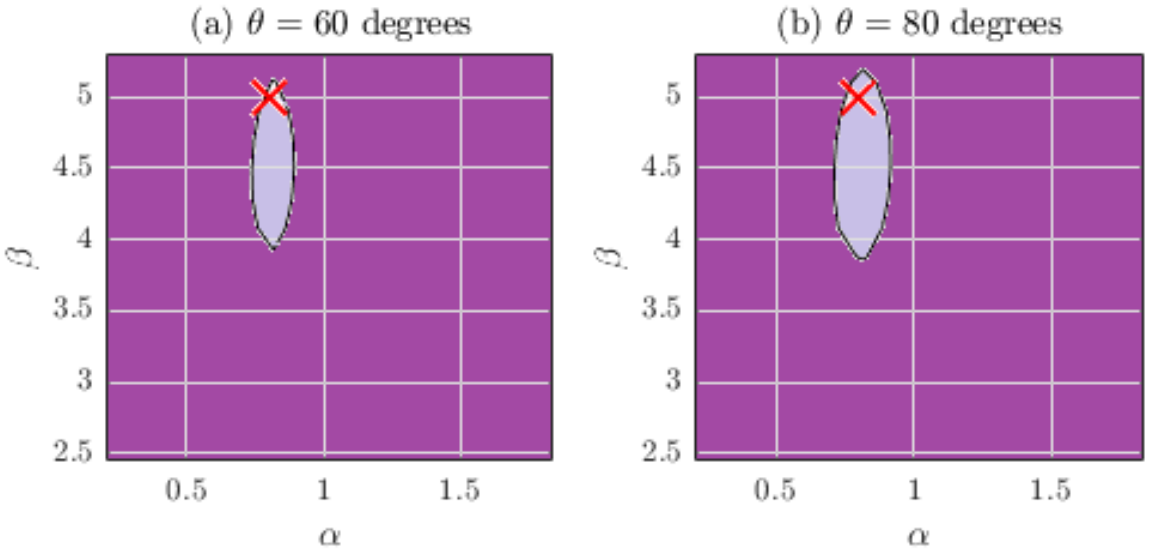

Figure 7.3: Neutral stability plots in the wavenumber state space for the pCf. The instability region is shown in light purple, with the dark purple region being the stable area. The red cross marks the most unstable point. The input parameters were $(Re, F_h) = (10000, 1)$ and (a) $\theta = 60$ degrees, (b) $\theta = 80$ degrees.

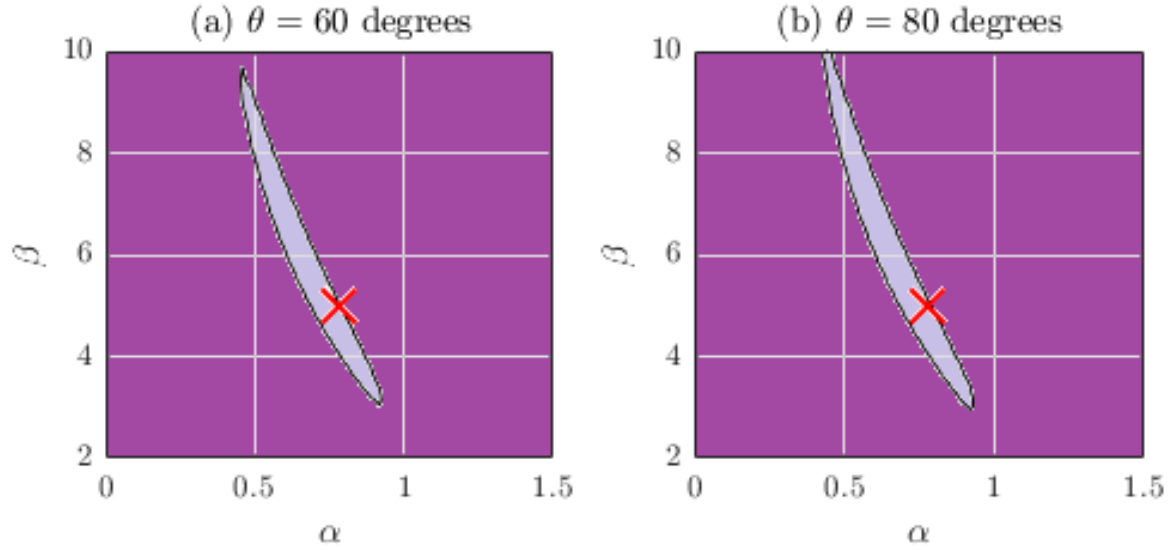

Figure 7.4: Neutral stability plots in the wavenumber state space for the pCf. The instability region is shown in light purple, with the dark purple region being the stable area. The red cross marks the most unstable point. The input parameters were $(Re, F_h) = (10000, 0.5)$ and (a) $\theta = 60$ degrees, (b) $\theta = 80$ degrees.

Now observing Figures 7.5 and 7.6 which were results for the pPf, there is a noticeably larger region of instability in the wavenumber state space with respect to the pCf. This is a particularly expected result as the unstratified pPf is more unstable than the pCf. Once again, by increasing the stratification (by reducing F_h), the region of instability grows, as found with the pCf. This can be seen as the unstable bubble is much larger for the respectively tilt angle between the two Figures.

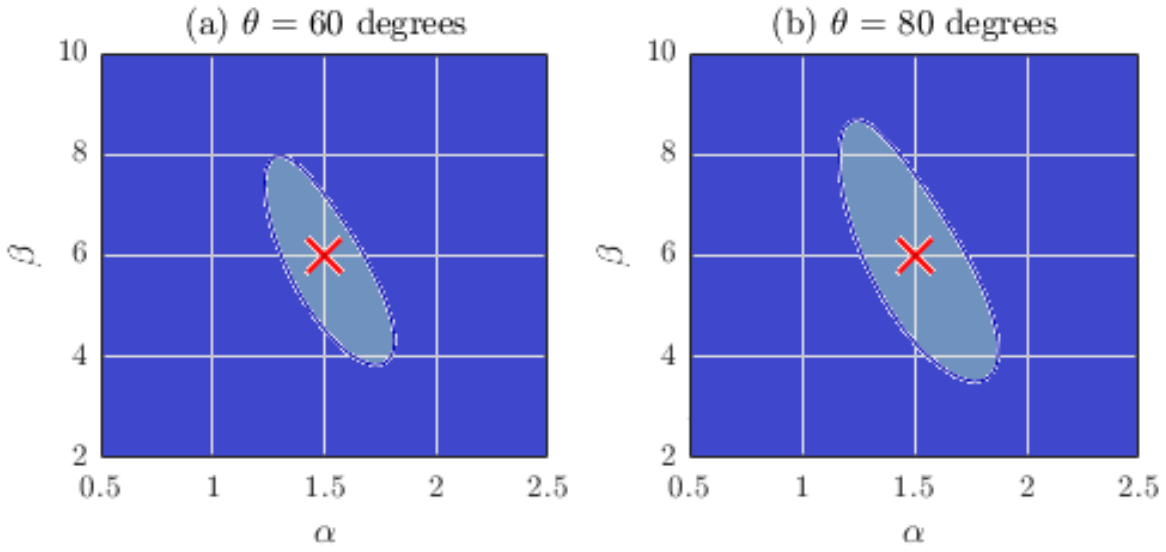

Figure 7.5: Neutral stability plots in the wavenumber state space for the pPf. The instability region is shown in light blue, with the dark blue region being the stable area. The red cross marks the most unstable point. The input parameters were $(Re, F_h) = (10000, 1)$ and (a) $\theta = 60$ degrees, (b) $\theta = 80$ degrees.

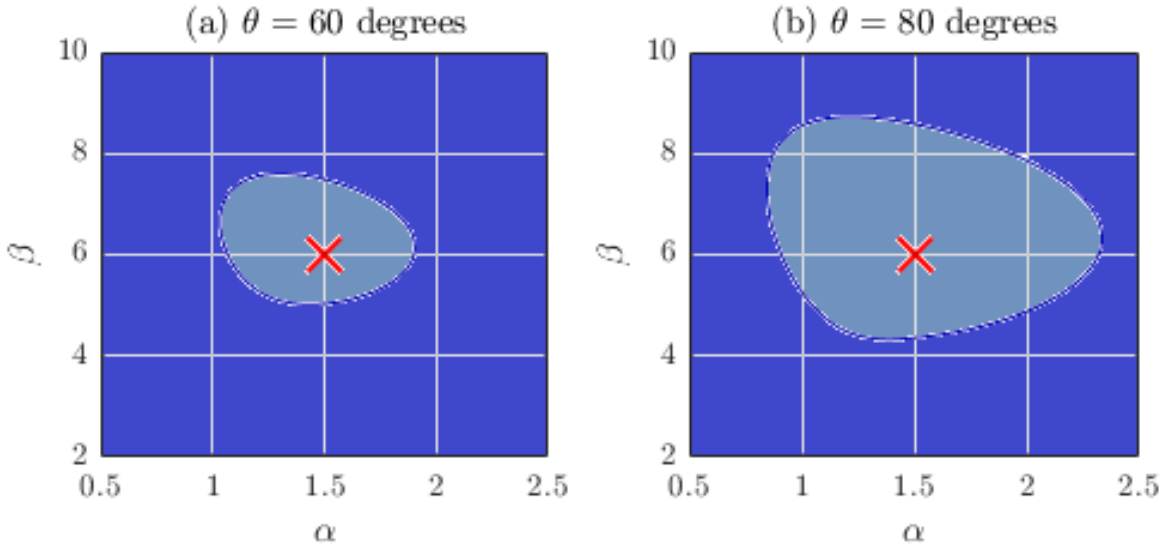

Figure 7.6: Neutral stability plots in the wavenumber state space for the pPf. The instability region is shown in light blue, with the dark blue region being the stable area. The red cross marks the most unstable point. The input parameters were $(Re, F_h) = (10000, 0.5)$ and (a) $\theta = 60$ degrees, (b) $\theta = 80$ degrees.

Likewise, as the tilt angle increases, the instability bubble grows. However, unlike the pCf, the most unstable region (marked with the red cross), is found around the centre of the instability region. This could suggests that at the critical tilt angle, the instability region is likely to be introduced at this point and then propagate in the wavenumber space as tilt angle is raised.

The most unstable region for the pCf was at the point $(\alpha, \beta) = (0.8, 5)$ (as found by Facchini) and $(1.5, 6)$ for the pPf.

7.3 General Reynolds Number Influences, *Re*

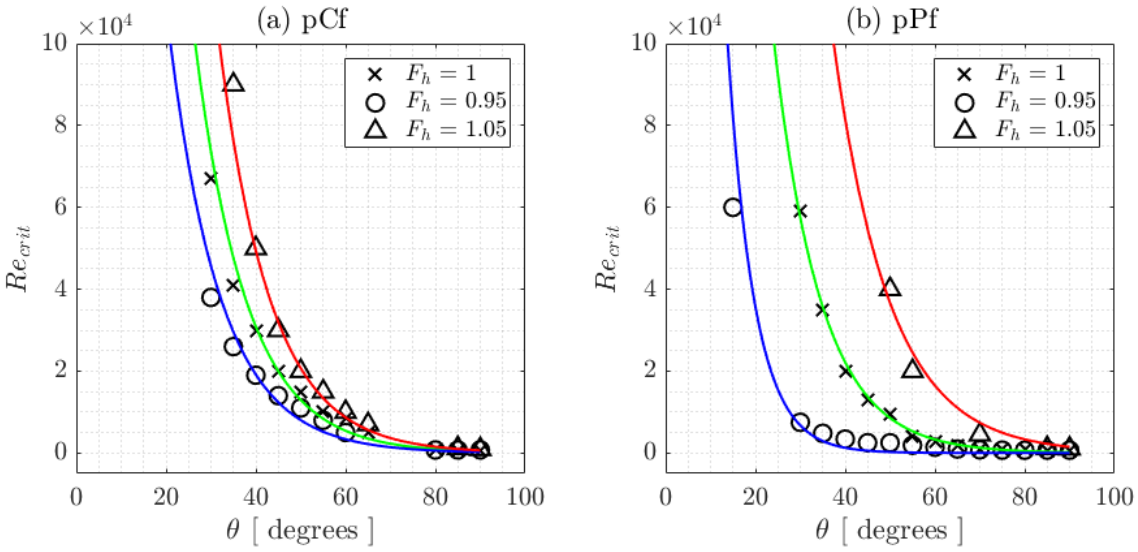

Figure 7.7: Caption

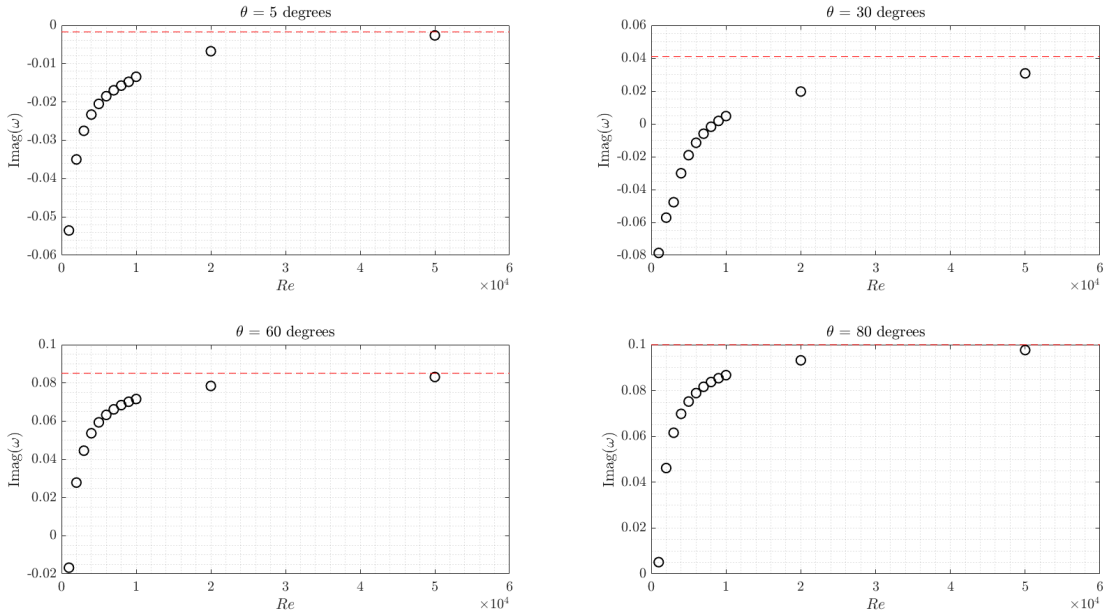

Figure 7.8: Caption

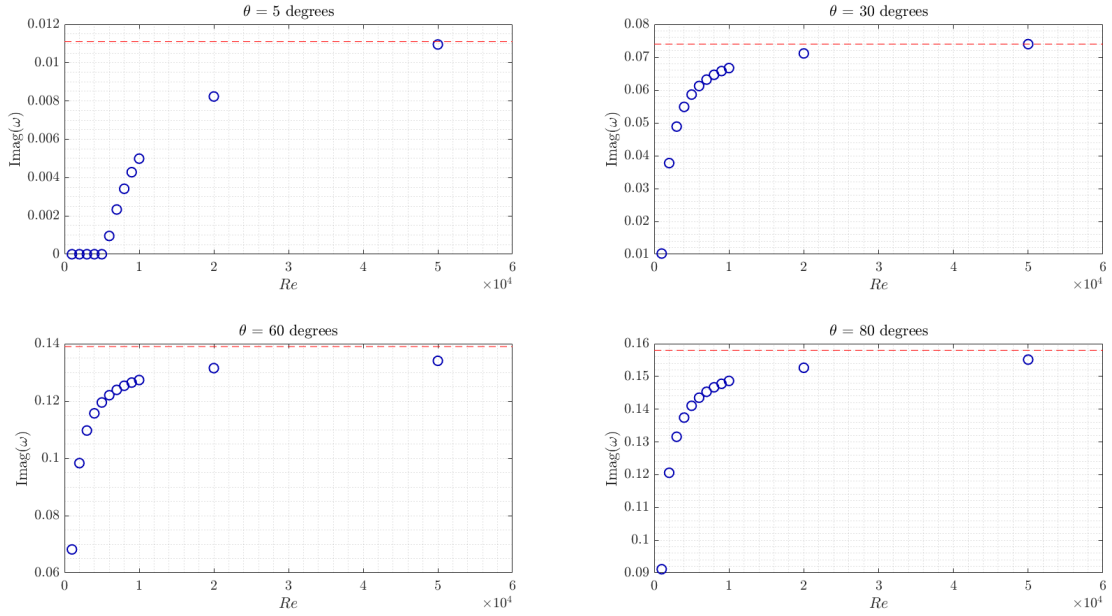

Figure 7.9: Caption

7.4 General Stratification Influences, F_h

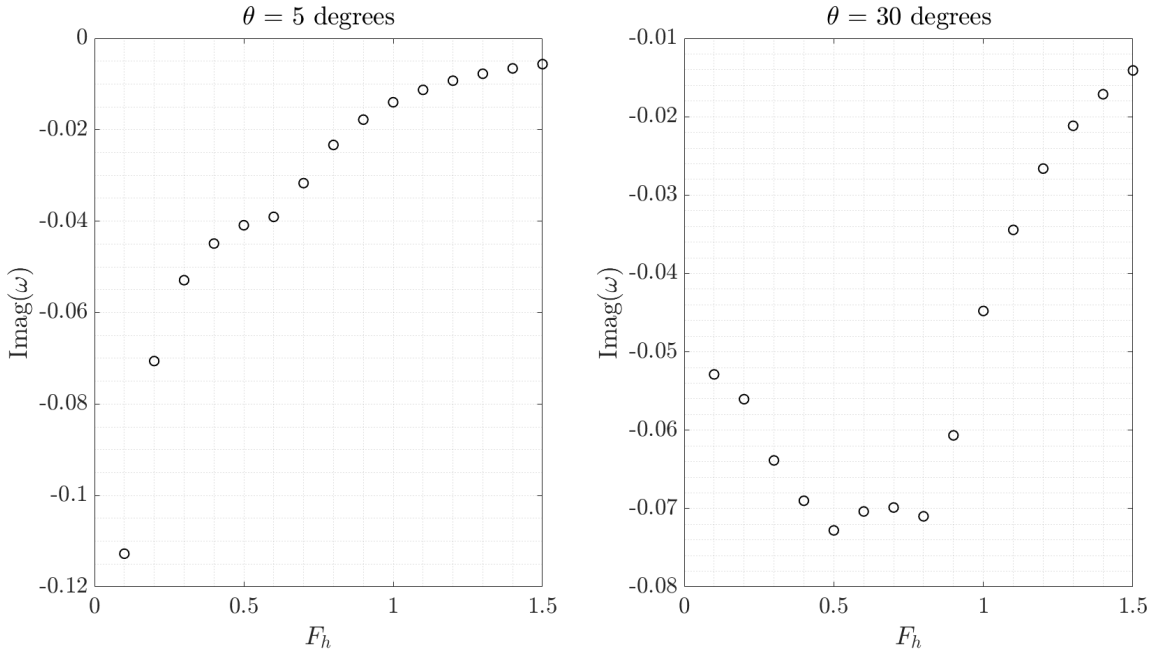

Figure 7.10: Caption

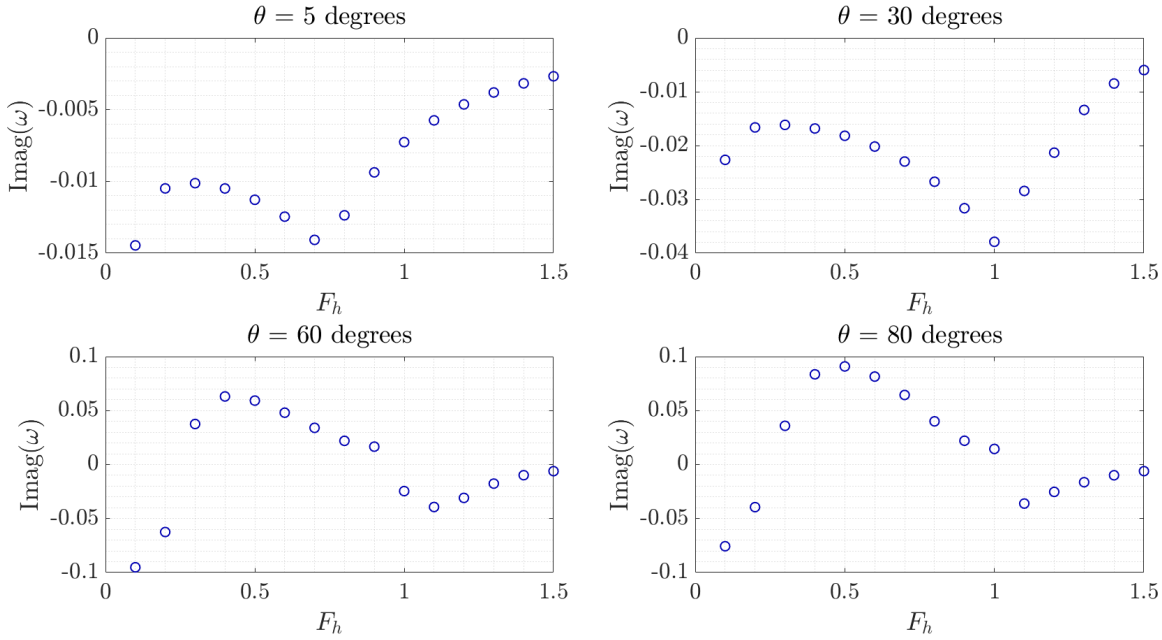

Figure 7.11: Caption

7.5 General Tilt Influences, θ

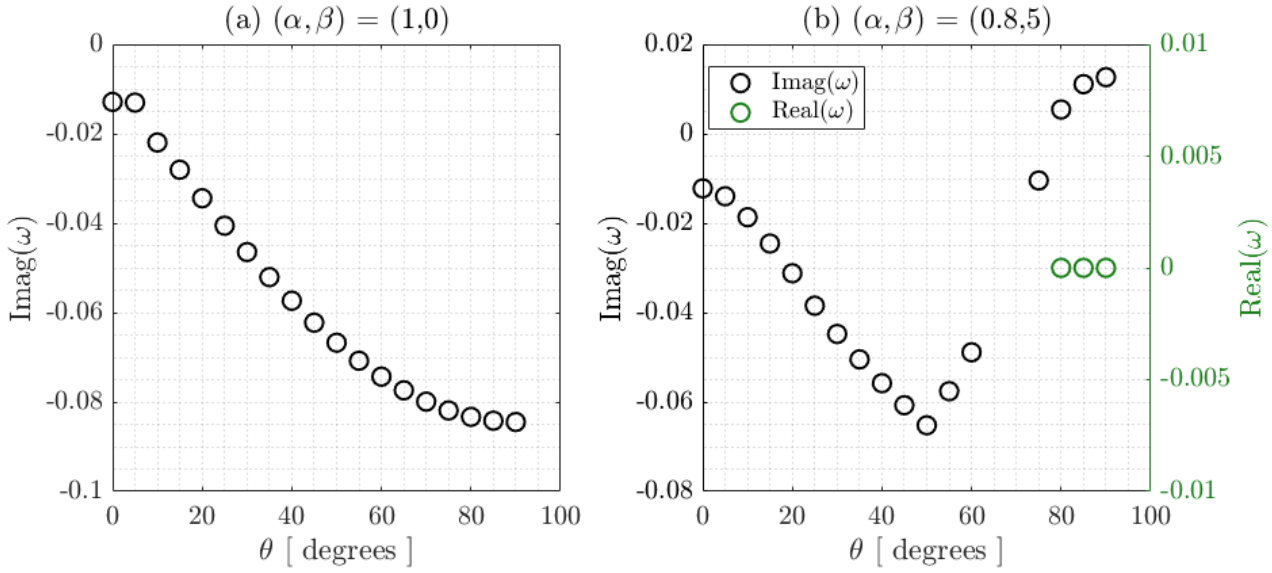

Figure 7.12: Caption

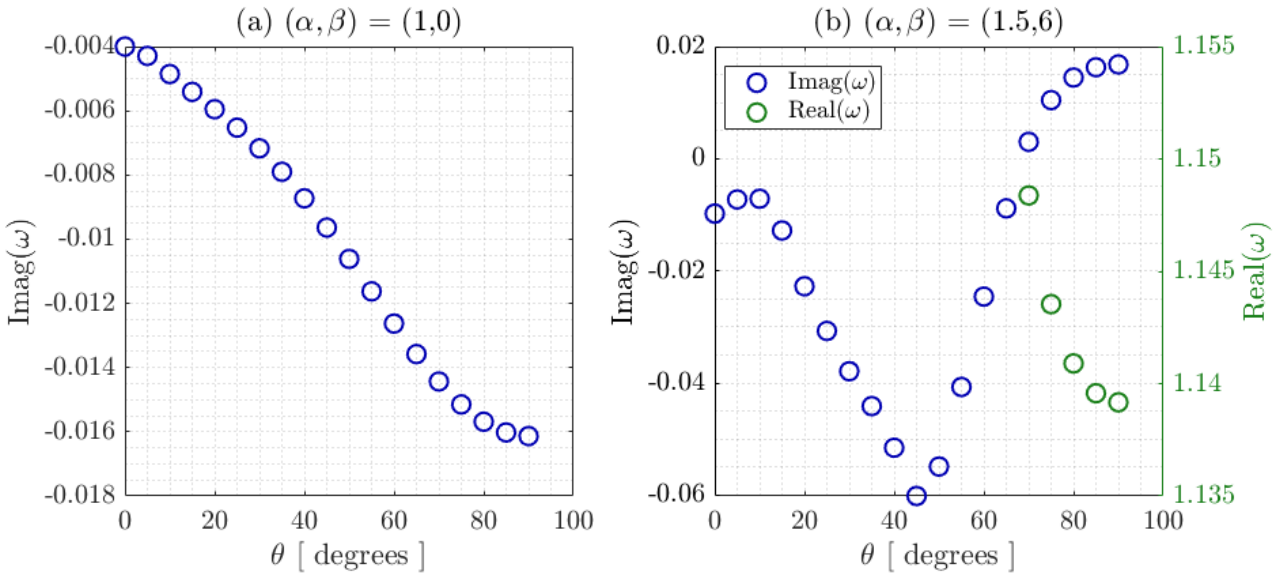

Figure 7.13: Caption

7.6 Eigenfunction

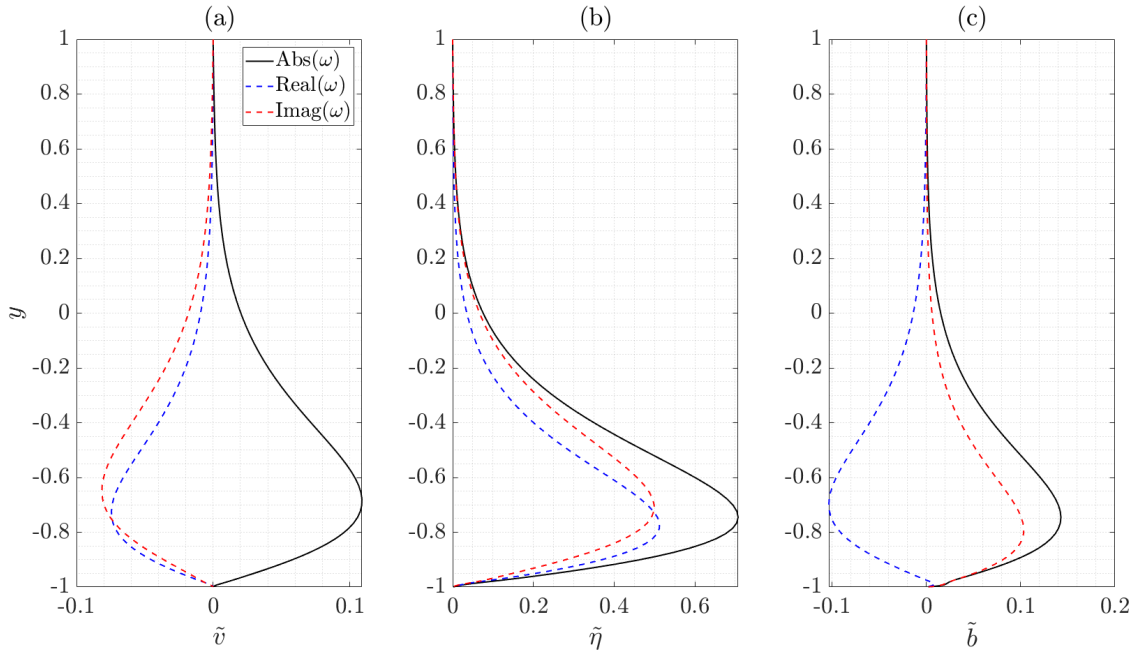

Figure 7.14: Caption

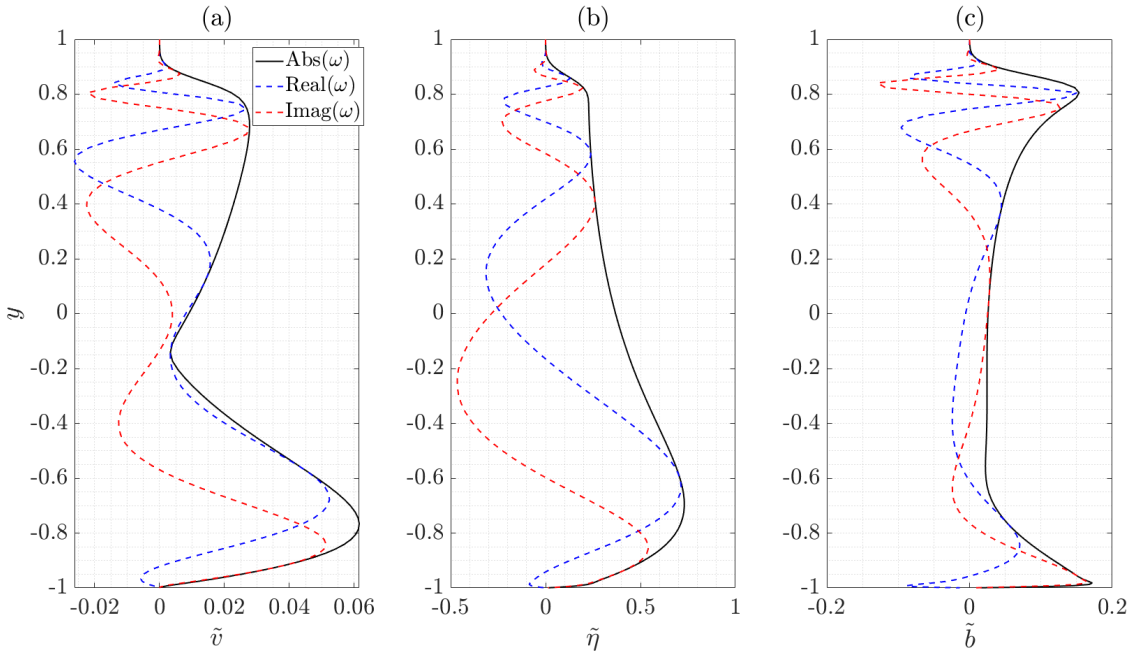

Figure 7.15: Caption

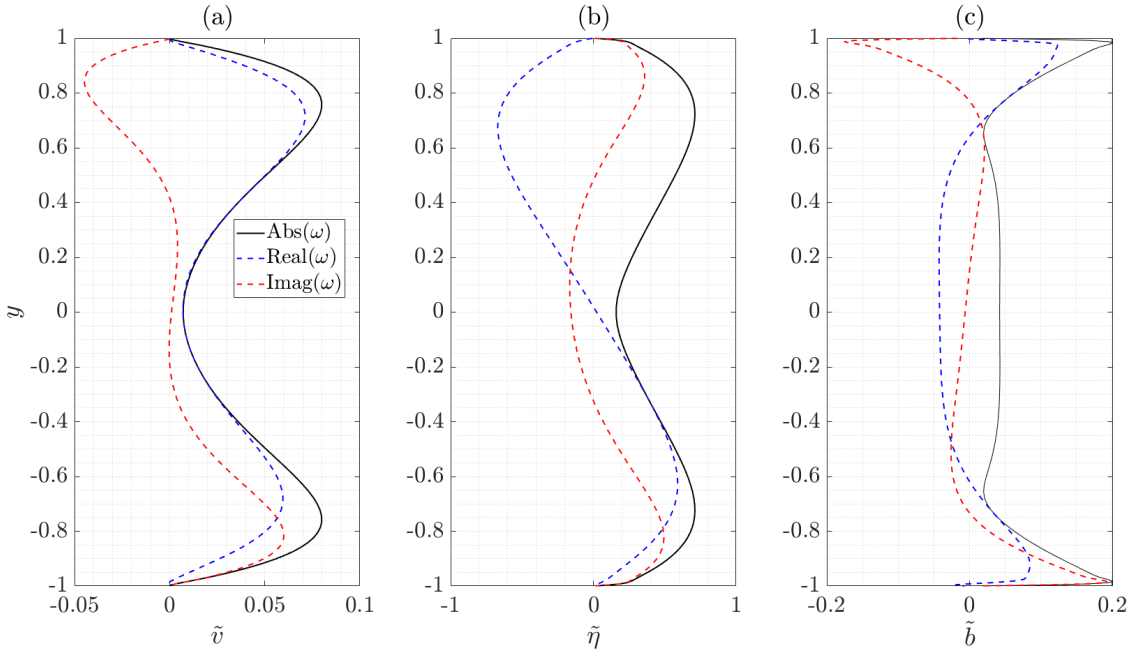

Figure 7.16: Caption

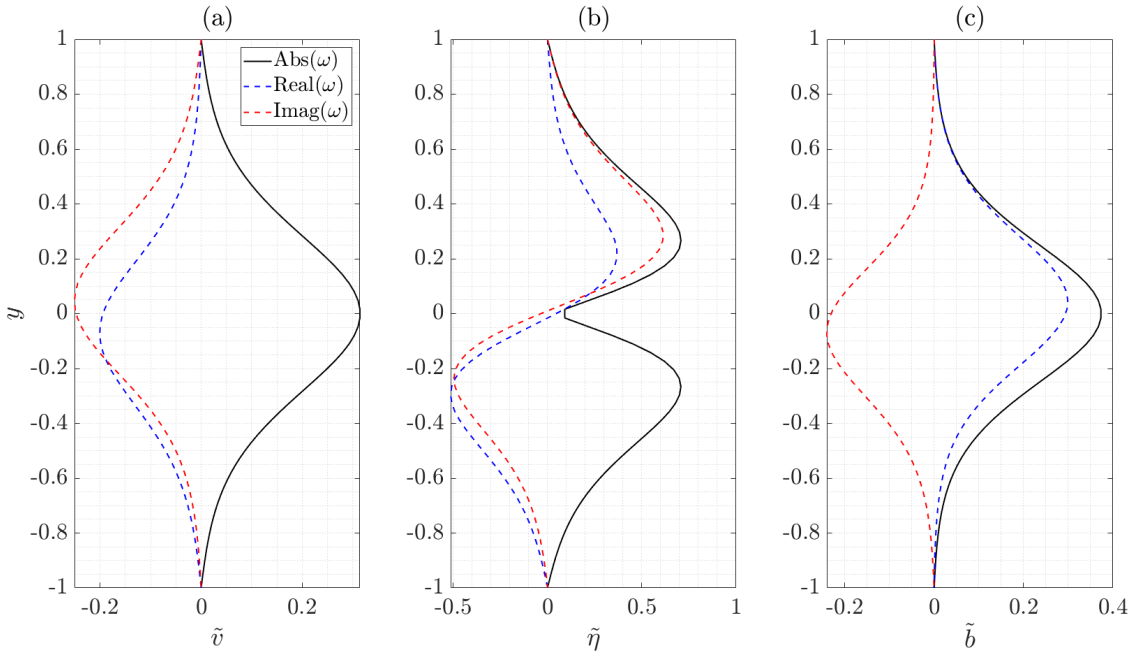

Figure 7.17: Caption

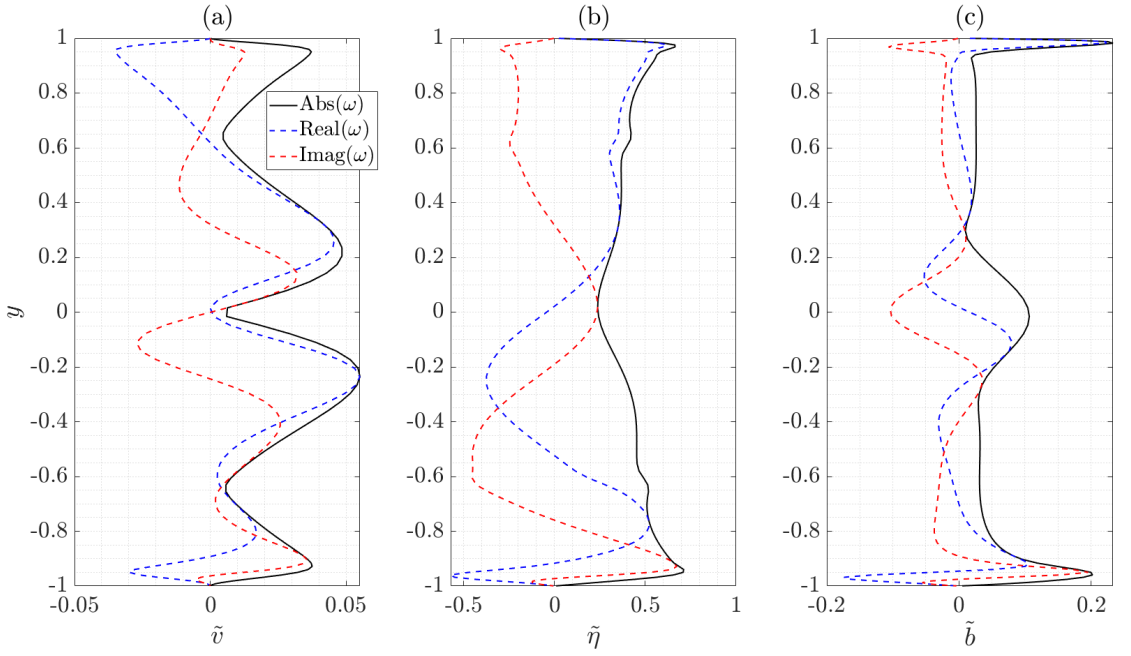

Figure 7.18: Caption

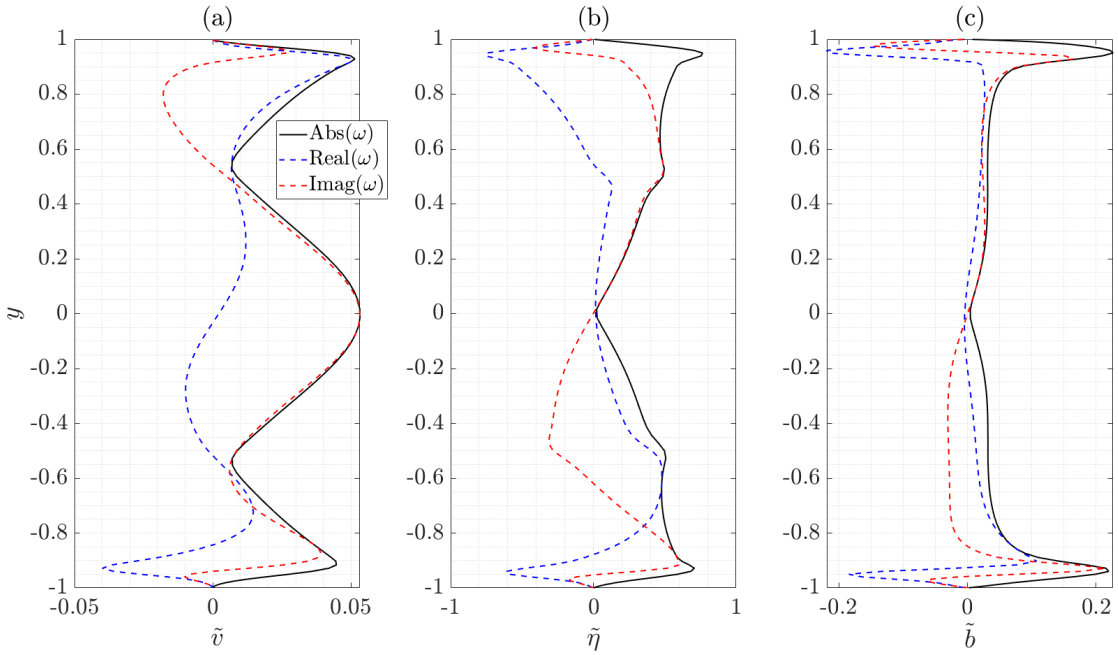

Figure 7.19: Caption

7.7 Effect Of Schmid Number, Sc

- Order of plots
  1. EIGENSPECTRA [x2] (1 effect of flow) **DONE**
  2. (A,B) SWEPT [x2] (2 effect of a,b) **DONE**
  3. THETA VS RE [x2] (3 effect of Re) **DONE**
  4. IMAG VS RE [x2] (3 effect of Re) **DONE**
  5. IMAG VS FH [x2] (4 effect of Fh) **DONE**
  6. IMAG VS THETA [x2] (5 effect of theta) **DONE**
  7. EIGENFUNCTION [x2] **DONE**
  8. AFFECT OF Sc **DONE**
- Plots basically the same for pCf and pPf remove and Appendix
- Consistent plots

Chapter 8

Conclusion

8.1 Conclusions

- **1 PAGE**

8.1.1 Future Work

- Non-linear stability analysis
- Implement Neumann boundary conditions
- More complete analysis of pPf/Other shear flows
- Investigate other density profiles
- Understand physics
- More tilt angles
- Neutral stability contours in the instability region

Appendix A

Appendix

A.1 MATLAB Solver

A.2 Chebyshev Solver

A.3 Stratified System Derivation

A.4 Code Flow Diagram

A.5 Grid Point Convergence

A.6 Full Validation

A.7 Aligned Cases Analysis